

Tree-Sliced Wasserstein Distance on a System of Lines

Viet-Hoang Tran^{†,*} Trang Pham^{◇,*} Tho Tran[†]
 Tam Le^{‡,‡,**} Tan M. Nguyen^{†,**}

National University of Singapore[†]

VinAI Research[◇]

The Institute of Statistical Mathematics[‡]

RIKEN AIP[‡]

June 21, 2024

Abstract

Sliced Wasserstein (SW) distance in Optimal Transport (OT) is widely used in various applications thanks to its statistical effectiveness and computational efficiency. On the other hand, Tree Wasserstein (TW) and Tree-sliced Wasserstein (TSW) are instances of OT for probability measures where its ground cost is a tree metric. TSW also has a low computational complexity, i.e. linear to the number of edges in the tree. Especially, TSW is identical to SW when the tree is a chain. While SW is prone to loss of topological information of input measures due to relying on one-dimensional projection, TSW is more flexible and has a higher degree of freedom by choosing a tree rather than a line to alleviate the curse of dimensionality in SW. However, for practical applications, popular tree metric sampling methods are heavily built upon given supports, which limits their capacity to adapt to new supports. In this paper, we propose the Tree-Sliced Wasserstein distance on a System of Lines (TSW-SL), which brings a connection between SW and TSW. Compared to SW and TSW, our TSW-SL benefits from the higher degree of freedom of TSW while being suitable to dynamic settings as SW. In TSW-SL, we use a variant of the Radon Transform to project measures onto a system of lines, resulting in measures on a space with a tree metric, then leverage TW to efficiently compute distances between them. We empirically verify the advantages of TSW-SL over the traditional SW by conducting a variety of experiments on gradient flows, image style transfer, and generative models.

1 Introduction

Optimal transport (OT) [48, 38] is a naturally geometrical metric for comparing probability distributions. Intuitively, OT lifts the ground cost metric among supports of input measures into the metric between two input measures. OT has been applied in many research fields, including machine learning [4, 47, 8, 13, 31], statistics [26, 50, 20, 35, 36, 49, 39], multimodal [37, 24], computer vision and graphics [41, 46, 17, 34, 43].

However, OT has a supercubic computational complexity concerning the number of supports in input measures [38]. To address this computational complexity issue, sliced-Wasserstein

* Co-first authors, ** Co-last authors

(SW) [3, 41] exploits the closed-form expression of the one-dimensional OT to reduce its complexity. In particular, SW projects supports of input measures onto a random line and leverages the fast computation of the OT on one dimension. SW is widely used in various applications, such as gradient flows [2, 21], clustering [15, 12], domain adaptation [5], generative models [7, 51, 30], thanks to its statistical effectiveness and computational efficiency. Due to relying on one-dimensional projection, SW limits its capacity to capture the topological structures of input measures, especially in high-dimensional application domains.

Previous works has been conducted to improve SW [29, 33, 31] or study variants of SW [1, 14, 40]. Recently, Tree-sliced Wasserstein (TSW) was proposed [19], which employs the tree structure to alleviate the loss of topological information of input measures since the tree structure is more flexible and has a higher degree of freedom than the line as in SW. Moreover, TSW can be considered as a generalization of SW since they are identical when the tree is a chain. Additionally, TSW yields a closed-form expression for a fast computation, which is linear to the number of nodes in the tree. However, in most practical applications, there is no prior tree structure, and sampling tree metric is an essential step for TSW. Popular tree metric sampling methods, e.g., partition-based such as QuadTree or clustering-based tree metric sampling methods [19], are heavily built upon given supports of input measures. Furthermore, the sampled tree is bounded, i.e., given leave nodes, one cannot go further away from the root beyond those leave nodes. This constraint limits TSW’s capacity to adapt to new supports, which is required for applications such as generative models and gradient flow.

Contribution. In summary, our contributions are three-fold:

1. We introduce the notion of a tree system which is a collection of lines (system of lines) with an additional tree structure. We study the topology of a tree system and provide a simple method for constructing and sampling tree systems. An important property of tree systems is, they are well-defined metric spaces with metrics are tree metrics. TW can be computed between measures supported on these spaces and becomes a metric on the space of measures. It also solves the bounded supports issue in existing tree metric sampling methods for TSW.
2. We define the space of integrable functions and probability measures on a tree system, and introduce a novel integral transform, called *Radon Transform on System of Lines*, which is a variant of traditional Radon Transform. This variant naturally transforms measures supported in high dimensional space onto tree systems instead of one line as Radon Transform, and is identical to Radon Transform in a special case. The injectivity of this variant holds as previous proposed Radon Transform variants.
3. We propose the Tree-Sliced Wasserstein distance on a System of Lines (TSW-SL), which brings a connection between SW and TW. Compared to SW and TW, ours has a closed-form expression for fast computation as SW and TW, and also benefits from the high degree of freedom of TW. We further propose MaxTSW-SL, which is an analog of Max Sliced Wasserstein (MaxSW).

We empirically verify the advantages of TSW-SL over the traditional SW, and variants of SW by conducting experiments on gradient flows [14], image style transfer [29], and generative models [7].

Organization. The remainder of the paper is organized as follows. Section 2 provides backgrounds of SW and TSW distances. Section 3 introduces the notion of tree systems and studies its properties, and Section 4 proposes the Radon Transform on System of Lines. Finally, we propose the Tree-Sliced Wasserstein distance on a System of Lines and its Max variant in Section 5. Finally, section 6 contains empirical results for TSW-SL. Formal constructions, theoretical proofs of key results, and additional materials are presented in the Appendix.

Notation. For $d > 0$, $\mathbb{S}^{d-1} := \{\theta \in \mathbb{R}^d : \|\theta\|_2 = 1\}$ denote the d -dimensional unit sphere with L^2 -norm. For sequences $\{a_n\}$ and $\{b_n\}$, the notation $a_n = \mathcal{O}(b_n)$ means that $a_n \leq C \cdot b_n$ for all $n > 0$ where C is a constant. Tree refers to a graph which is a tree, i.e. graph that exists one and only one path between every two of its nodes.

2 Preliminaries

In this section, we review Sliced Wasserstein (SW) and Tree Sliced Wasserstein (TSW) distances.

2.1 Sliced Wasserstein Distance

Wasserstein Distance. Let Ω be a measurable space endowed with a metric d , and μ, ν be two Borel probability distributions on Ω . Let $\mathcal{P}(\mu, \nu)$ be the set of probability distributions π on the product space $\Omega \times \Omega$ such that $\pi(A \times \Omega) = \mu(A)$ and $\pi(\Omega \times B) = \nu(B)$ for all Borel sets A, B . For $p \geq 1$, the p -Wasserstein distance ($W_{d,p}$) [48] between μ, ν is defined as:

$$W_{d,p}(\mu, \nu) = \inf_{\pi \in \mathcal{P}(\mu, \nu)} \left(\mathbb{E}_{(x,y) \sim \pi} [d(x,y)^p] \right)^{\frac{1}{p}}. \quad (1)$$

Sliced Wasserstein Distance. For $p \geq 1$, the p -order Sliced Wasserstein (SW) distance [3] between two probability distributions μ, ν is defined by:

$$\text{SW}_p(\mu, \nu) := \left(\mathbb{E}_{\theta \sim \mathcal{U}(\mathbb{S}^{d-1})} [W_p^p(\theta \# \mu, \theta \# \nu)] \right)^{\frac{1}{p}}, \quad (2)$$

where $W_p(\theta \# \mu, \theta \# \nu)$ is the one-dimensional p -Wasserstein distance between the projections of μ and ν along direction θ , which has the closed-form $W_p^p(\theta \# \mu, \theta \# \nu) = \int_0^1 |F_{\theta \# \mu}^{-1}(z) - F_{\theta \# \nu}^{-1}(z)|^p dz$, where $F_{\theta \# \mu}$ and $F_{\theta \# \nu}$ are the cumulative distribution functions of $\theta \# \mu$ and $\theta \# \nu$.

Monte Carlo estimation for SW. Monte Carlo method is often used to estimate the expectation approximate the intractable expectation in Eq. (2) as follows:

$$\widehat{\text{SW}}_p(\mu, \nu; L) = \left(\frac{1}{L} \sum_{l=1}^L W_p^p(\theta_l \# \mu, \theta_l \# \nu) \right)^{\frac{1}{p}}, \quad (3)$$

Max Sliced Wasserstein (MaxSW) distance is discussed in Appendix D.

where $\theta_1, \dots, \theta_L \stackrel{\text{i.i.d.}}{\sim} \mathcal{U}(\mathbb{S}^{d-1})$. When μ and ν are discrete measures that have at most N supports in d dimensions, the time complexity to compute $\widehat{\text{SW}}_p$ is $\mathcal{O}(LN \log N + LdN)$. Here, $\mathcal{O}(LN \log N)$ is for sorting L sets of supports after projecting, and $\mathcal{O}(LdN)$ is for projecting supports to L sets of scalars.

2.2 Tree Sliced Wasserstein Distance and Sobolev Transport

A metric $d: \Omega \times \Omega \rightarrow [0, \infty)$ is called a *tree metric* on Ω if there exists a tree \mathcal{T} with Ω is its node set and non-negative edge lengths such that for every $x, y \in \Omega$, $d(x, y)$ equals to the length of the (unique) path between x and y [45]. We write the tree metric corresponding to that tree $d_{\mathcal{T}}$, and denote the p -Wasserstein distance with ground metric $d_{\mathcal{T}}$ as in Eq. (1) as $W_{d_{\mathcal{T}}, p}$.

Tree Wasserstein Distances. For $p = 1$, the 1-Wasserstein distance $W_{d_{\mathcal{T}}, 1}$ admits a closed-form [22, 23]. More concretely, let \mathcal{T} be a tree with non-negative edge lengths, and given two measures μ, ν supported on nodes of \mathcal{T} , and the ground metric $d_{\mathcal{T}}$, i.e. the length of the (unique) path between two points. The Wasserstein distance with ground metric $d_{\mathcal{T}}$ (TW) [19] has closed-form as follows:

$$W_{d_{\mathcal{T}}, 1}(\mu, \nu) = \sum_{e \in \mathcal{T}} w_e \cdot |\mu(\Gamma(v_e)) - \nu(\Gamma(v_e))|. \quad (4)$$

where v_e is one of the node of edge e and farther away from the tree root, $\Gamma(v_e)$ is a subtree rooted at v_e , and w_e is the length of edge e . When there are multiple tree metrics on \mathcal{T} , Tree Sliced Wasserstein (TSW) is an average of TW on each tree metric [19]. It is worth noting that the closed-form expression of TW only holds for $p = 1$. When $p > 1$, it is unknown whether one can compute $W_{d_{\mathcal{T}}, p}$ efficiently.

Sobolev Transport. Sobolev transport (ST) [18] leverages the Sobolev structure to generalize TW to any other $p \geq 1$ and still yields closed-form expression for fast computation. Indeed, for $p \geq 1$:

$$\text{ST}_{d_{\mathcal{T}}, p}(\mu, \nu) = \left(\sum_{e \in \mathcal{T}} w_e \cdot |\mu(\Gamma(v_e)) - \nu(\Gamma(v_e))|^p \right)^{\frac{1}{p}}. \quad (5)$$

When $p = 1$, ST is equal to TW, i.e. $\text{ST}_{d_{\mathcal{T}}, 1}(\mu, \nu) = W_{d_{\mathcal{T}}, 1}(\mu, \nu)$ for μ, ν supported on tree \mathcal{T} .

3 System of Lines with Tree Structures

In this section, we will introduce the notion of a finite system of lines. We also introduce the notion of tree structures of systems of lines, which form a tree system, and then discuss the topological properties and the construction of a tree system. We will briefly describe the concepts with visualizations as in Figure 1, 2, 3.

A complete formal construction and theoretical proofs are deferred in Appendix A.

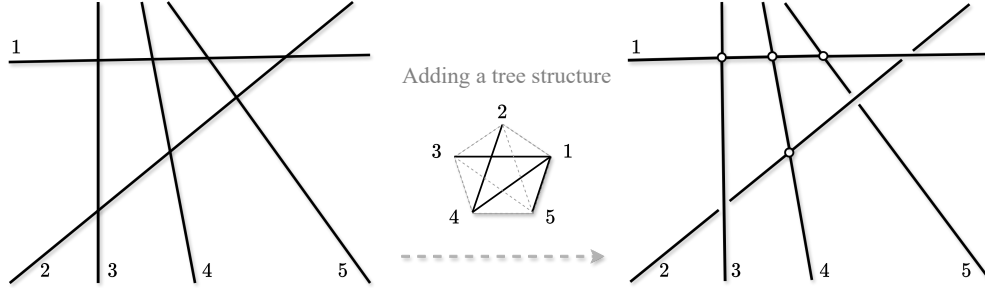


Figure 1: Illustration of how to add a tree structure to a system of lines. *Left*: An example of a system of 5 lines in \mathbb{R}^2 . Here, they intersect each other, so the system is connected. *Right*: Adding a tree structure to the connected system. In our example, only four pairs of lines are adjacent (presented by intersections), and others are not (presented by gaps). This comes from taking a spanning tree of the graph with 5 nodes represented for 5 lines, with edges represented if the two lines intersect or not.

3.1 System of Lines and Tree System

We have an observation of a line parameterized by its direction and a point it passes through: A line in \mathbb{R}^d is completely determined by a pair $(x, \theta) \in \mathbb{R}^d \times \mathbb{S}^{d-1}$ via $x + t \cdot \theta, t \in \mathbb{R}$.

Definition 3.1 (Line and System of lines in \mathbb{R}^d). A *line* in \mathbb{R}^d is an element (x, θ) of $\mathbb{R}^d \times \mathbb{S}^{d-1}$. For $n \geq 1$, a *system of n lines* in \mathbb{R}^d is a set of n lines in \mathbb{R}^d .

We denote a line in \mathbb{R}^d as $l = (x_l, \theta_l)$. Here, x_l and θ_l are called *source* and *direction* of l , respectively. Denote $(\mathbb{R}^d \times \mathbb{S}^{d-1})^n$ by \mathbb{L}_n^d , which is the *collection of systems of n lines* in \mathbb{R}^d , and an element of \mathbb{L}_n^d is usually denoted by \mathcal{L} . The *ground set* of a system of lines \mathcal{L} is defined by:

$$\bar{\mathcal{L}} := \left\{ (x, l) \in \mathbb{R}^d \times \mathcal{L} : x = x_l + t_x \cdot \theta_l \text{ for some } t_x \in \mathbb{R} \right\}.$$

For each element $\bar{\mathcal{L}}$, we sometimes write (x, l) as (t_x, l) , where $t_x \in \mathbb{R}$ presents the parameterization of x on l as $x = x_l + t_x \cdot \theta_l$. By a point of \mathcal{L} , we refer to a point of the ground set $\bar{\mathcal{L}}$.

Now consider a system of distinct lines \mathcal{L} in \mathbb{R}^d . \mathcal{L} is called *connected* if its points form a connected set in \mathbb{R}^d . In this case, \mathcal{L} naturally has some tree structures. Figure 1 gives an example of a system of lines and adding a tree structure to the system. A pair $(\mathcal{L}, \mathcal{T})$ consists of a connected system of lines \mathcal{L} and a tree structure \mathcal{T} of \mathcal{L} is called a *tree system*. We also write it as \mathcal{L} for short.

3.2 Topological Properties of Tree Systems

Intuitively, a tree system \mathcal{L} is a collection of some lines that connect to each other in some ways. It naturally forms a topological space by taking disjoint union copies of \mathbb{R} and then taking the quotient at intersections of these copies. The disjoint union is straightforward, and the quotient will follow the tree structure of \mathcal{L} . The topological space resulting from these actions

is called by *topological space of a tree system* \mathcal{L} , and is denoted by $\Omega_{\mathcal{L}}$. By its construction, $\Omega_{\mathcal{L}}$ naturally has a measure that is induced from the usual measure on each copy of \mathbb{R} . We denote this measure by $\mu_{\mathcal{L}}$.

Observe that, from the tree structure, there exists a *unique* path between two points of $\Omega_{\mathcal{L}}$. By this, we have an important result about the metrizable of $\Omega_{\mathcal{L}}$.

Theorem 3.2 ($\Omega_{\mathcal{L}}$ is metrizable by a tree metric). *Consider $d_{\mathcal{L}}: \Omega_{\mathcal{L}} \times \Omega_{\mathcal{L}} \rightarrow [0, \infty)$ defined by:*

$$d_{\mathcal{L}}(a, b) := \mu_{\mathcal{L}}(P_{a,b}) \text{ , } \forall a, b \in \Omega_{\mathcal{L}}, \quad (6)$$

where $P_{a,b}$ is the unique path between a and b in $\Omega_{\mathcal{L}}$. Then $d_{\mathcal{L}}$ is a metric on $\Omega_{\mathcal{L}}$, which makes $(\Omega_{\mathcal{L}}, d_{\mathcal{L}})$ a metric space. Moreover, $d_{\mathcal{L}}$ is a tree metric, and the topology on $\Omega_{\mathcal{L}}$ induced by $d_{\mathcal{L}}$ is identical to the topology of $\Omega_{\mathcal{L}}$.

The proof is provided in Theorem A.11. Figure 2 gives an example of a unique path between two points lying on a tree system and intuitively shows why $d_{\mathcal{L}}$ is indeed a metric.

3.3 Construction of Tree Systems and Sampling

A tree system can be inductively constructed by sampling lines as long as each line has to intersect one of the previous lines. Here we present a simple way to construct a tree system by, sampling a line at first, then at each step, sampling one line that intersects the previous line. More specifically:

Step 1. Sampling $x_1 \sim \mu_1$ for an $\mu_1 \in \mathcal{P}(\mathbb{R}^d)$, then $\theta_1 \sim \nu_1$ for an $\nu_1 \in \mathcal{P}(\mathbb{S}^{d-1})$. The pair (x_1, θ_1) forms the first line;

Step i . At step i , sampling $x_i = x_{i-1} + t_i \cdot \theta_{i-1}$ where $t_i \sim \mu_i$ for an $\mu_i \in \mathcal{P}(\mathbb{R})$, then $\theta_i \sim \nu_i$ for an $\nu_i \in \mathcal{P}(\mathbb{S}^{d-1})$. The pair (x_i, θ_i) forms the i^{th} line.

The collection of lines obtained by this construction has the tree structure as a chain, where the i^{th} line intersects the $(i+1)^{\text{th}}$ line. We present how to sample a general tree system in Appendix A.4. In practice, we simply assume all the distributions μ 's and ν 's to be independence, and let:

1. μ_1 to be a distribution on a bounded subset of \mathbb{R}^d , for instance, the uniform distribution on the d -dimensional cube $[-1, 1]^d$, i.e. $\mathcal{U}([-1, 1]^d)$;
2. μ_i for $i > 1$ to be a distribution on a bounded subset of \mathbb{R} , for instance, the uniform distribution on the interval $[-1, 1]$, i.e. $\mathcal{U}([-1, 1])$;
3. θ_n to be a distribution on \mathbb{S}^{d-1} , for instance, the uniform distribution $\mathcal{U}(\mathbb{S}^{d-1})$;

By μ 's and ν 's, we get a distribution on the space of all tree systems that can be sampled by this way. We summarize the sampling tree systems algorithm by Algorithm 1 and Figure 3.

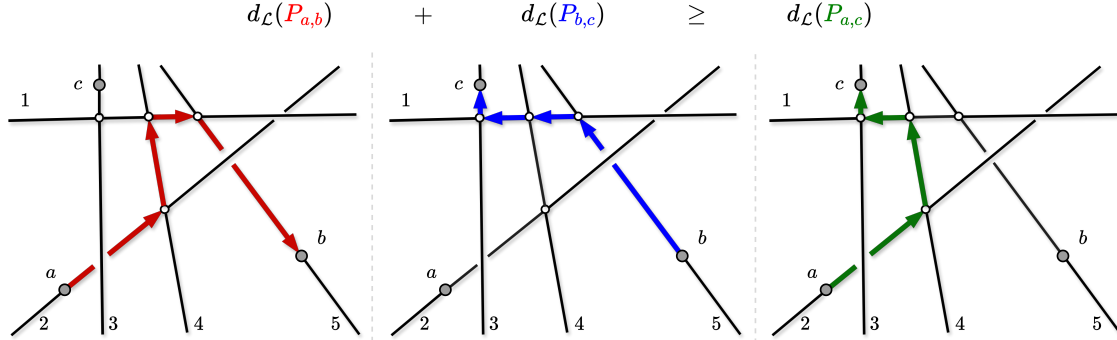


Figure 2: The same tree system \mathcal{L} as in Figure 1. It naturally has a topology that arises from five copies of \mathbb{R} . Consider three points a, b, c . The red zigzag line presents the unique path from a to b . Here the distance between a, b , i.e. $d_{\mathcal{L}}(a, b)$, is the sum of four red line segments. Similar for paths between b and c , a and c . The inequality shows the triangle inequality holds for $d_{\mathcal{L}}$.

Algorithm 1 Sampling a tree system.

Input: The number of lines in tree systems n .
Sampling $x_1 \sim \mathcal{U}([-1, 1]^d)$ and $\theta_1 \sim \mathcal{U}(\mathbb{S}^{d-1})$.

for $i = 2$ to N **do**

 Sample $t_i \sim \mathcal{U}([-1, 1])$ and $\theta_i \sim \mathcal{U}(\mathbb{S}^{d-1})$.

 Compute $x_i = x_{i-1} + t_i \cdot \theta_{i-1}$.

end for

Return: $(x_1, \theta_1), (x_2, \theta_2), \dots, (x_n, \theta_n)$.

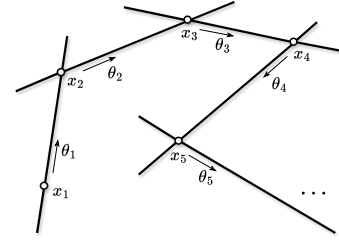


Figure 3: Illustration of Algorithm 1

4 Space of Integrable Functions on a System of Lines

In this section, we introduce the notions of the space of Lebesgue integrable functions and the Radon Transform for a system of lines. Let \mathcal{L} be a system of n lines. Denote $L^1(\mathbb{R}^d)$ as the space of Lebesgue integrable functions on \mathbb{R}^d with norm $\|\cdot\|_1$:

$$L^1(\mathbb{R}^d) = \left\{ f: \mathbb{R}^d \rightarrow \mathbb{R} : \|f\|_1 = \int_{\mathbb{R}^d} |f(x)| dx < \infty \right\}. \quad (7)$$

Two functions $f_1, f_2 \in L^1(\mathbb{R}^d)$ are considered to be identical if $f_1(x) = f_2(x)$ for almost everywhere on \mathbb{R}^d . As a counterpart, a *Lebesgue integrable function on \mathcal{L}* is a function $f: \bar{L} \rightarrow \mathbb{R}$ such that:

$$\|f\|_{\mathcal{L}} := \sum_{l \in \mathcal{L}} \int_{\mathbb{R}} |f(t_x, l)| dt_x < \infty. \quad (8)$$

The space of Lebesgue integrable functions on \mathcal{L} is denoted by $L^1(\mathcal{L})$. Two functions $f_1, f_2 \in L^1(\mathcal{L})$ are considered to be identical if $f_1(x) = f_2(x)$ for almost everywhere on $\bar{\mathcal{L}}$. The space $L^1(\mathcal{L})$ with norm $\|\cdot\|_{\mathcal{L}}$ is a Banach space.

Recall that \mathcal{L} has n lines. Denote the $(n-1)$ -dimensional standard simplex as $\Delta_{n-1} = \{(a_l)_{l \in \mathcal{L}} : \sum_{l \in \mathcal{L}} a_l = 1\} \subset \mathbb{R}^n$. Denote $\mathcal{C}(\mathbb{R}^d, \Delta_{n-1})$ as the space of continuous function from \mathbb{R}^d to Δ_{n-1} , and called a function in $\mathcal{C}(\mathbb{R}^d, \Delta_{n-1})$ by a *splitting*. Let \mathcal{L} be a system of lines in \mathbb{L}_n^d , α be a splitting in $\mathcal{C}(\mathbb{R}^d, \Delta_{n-1})$, we define an operator associated to α that transforms a Lebesgue integrable functions on \mathbb{R}^d to a Lebesgue integrable functions on \mathcal{L} , which is an analog of the usual Radon Transform. For $f \in \mathcal{P}(\mathbb{R}^d)$, define:

$$\mathcal{R}_{\mathcal{L}}^{\alpha} f : \bar{\mathcal{L}} \longrightarrow \mathbb{R} \quad (9)$$

$$(x, l) \longmapsto \int_{\mathbb{R}^d} f(y) \cdot \alpha(y)_l \cdot \delta(t_x - \langle y - x_l, \theta_l \rangle) dy, \quad (10)$$

where δ is the 1-dimensional Dirac delta function. For $f \in L^1(\mathbb{R}^d)$, we can show that $\mathcal{R}_{\mathcal{L}}^{\alpha} f \in L^1(\mathcal{L})$. Moreover, we have $\|\mathcal{R}_{\mathcal{L}}^{\alpha} f\|_{\mathcal{L}} \leq \|f\|_1$. In other words, the operator $\mathcal{R}_{\mathcal{L}}^{\alpha} : L^1(\mathbb{R}^d) \rightarrow L^1(\mathcal{L})$ is well-defined, and is a linear operator. The proof is provided in Theorem B.2. We present the variant of Radon transform for a system of lines.

Definition 4.1 (Radon Transform on system of lines). For $\alpha \in \mathcal{C}(\mathbb{R}^d, \Delta_{n-1})$, the operator \mathcal{R}^{α} :

$$\begin{aligned} \mathcal{R}^{\alpha} : L^1(\mathbb{R}^d) &\longrightarrow \prod_{\mathcal{L} \in \mathbb{L}_n^d} L^1(\mathcal{L}) \\ f &\longmapsto (\mathcal{R}_{\mathcal{L}}^{\alpha} f)_{\mathcal{L} \in \mathbb{L}_n^d}. \end{aligned}$$

is called the *Radon transform on a system of lines*.

Remark. If $n = 1$, there is only one splitting function which is the constants function 1, and the Radon Transform on \mathbb{L}_1^d is the same as the usual Radon Transform.

Many variants of the Radon transform requires the transform to be injective. In the case of systems of lines, the injectivity also holds for \mathcal{R}^{α} .

Theorem 4.2. \mathcal{R}^{α} is injective.

The proof of this theorem is provided in Theorem B.1. Denote $\mathcal{P}(\mathbb{R}^d)$ as the space of all probability distribution on \mathbb{R}^d , and define a *probability distribution on \mathcal{L}* to be a function $f \in L^1(\mathcal{L})$ such that $f : \bar{\mathcal{L}} \rightarrow [0, \infty)$ and $\|f\|_{\mathcal{L}} = 1$. The *space of probability distribution on \mathcal{L}* is denoted by $\mathcal{P}(\mathcal{L})$. We can show that the transform $\mathcal{R}_{\mathcal{L}}^{\alpha}$ transforms a distribution in $\mathcal{P}(\mathbb{R}^d)$ to a distribution on $\mathcal{P}(\mathcal{L})$. In other words, the restriction $\mathcal{R}_{\mathcal{L}}^{\alpha} : \mathcal{P}(\mathbb{R}^d) \rightarrow \mathcal{P}(\mathcal{L})$ is also well-defined.

5 Tree-Sliced Wasserstein Distance on System of Lines (TSW-SL)

In this section, we present our Tree-Sliced Wasserstein distance variant on System of Lines (TSW-SL). We consider \mathbb{T} as the space of all tree systems consisting of n lines in \mathbb{R}^d that can be sampled by Algorithm 1. By the remark at the end of Subsection 3.3, we have a *distribution σ on the space \mathbb{T}* . General cases of \mathbb{T} , as in Appendix A.4, will be treated similarly.

5.1 Tree-Sliced Wasserstein Distance

Fix a splitting function α in $\mathcal{C}(\mathbb{R}^d, \Delta_{n-1})$. Consider two probability distributions μ, ν in $\mathcal{P}(\mathbb{R}^d)$ and a tree system $\mathcal{L} \in \mathbb{T}$. By the Radon Transform $\mathcal{R}_{\mathcal{L}}^{\alpha}$ in Definition 4.1, μ and ν transform to two probability distributions $\mathcal{R}_{\mathcal{L}}^{\alpha}\mu$ and $\mathcal{R}_{\mathcal{L}}^{\alpha}\nu$ in $\mathcal{P}(\mathcal{L})$. By Theorem 3.2, \mathcal{L} has a tree metric $d_{\mathcal{L}}$, so we can compute p -Wasserstein distance $W_{d_{\mathcal{L}},p}(\mathcal{R}_{\mathcal{L}}^{\alpha}\mu, \mathcal{R}_{\mathcal{L}}^{\alpha}\nu)$ between $\mathcal{R}_{\mathcal{L}}^{\alpha}\mu$ and $\mathcal{R}_{\mathcal{L}}^{\alpha}\nu$ by Eq. (4).

Definition 5.1 (Tree-Sliced Wasserstein Distance on System of Lines). For $p \geq 1$, the *Tree-Sliced p -Wasserstein Distance on System of Lines* between μ, ν in $\mathcal{P}(\mathbb{R}^d)$ is defined by:

$$\text{TSW-SL}_p(\mu, \nu) := \left(\mathbb{E}_{\mathcal{L} \sim \sigma} \left[W_{d_{\mathcal{L}},p}^p(\mathcal{R}_{\mathcal{L}}^{\alpha}\mu, \mathcal{R}_{\mathcal{L}}^{\alpha}\nu) \right] \right)^{\frac{1}{p}}. \quad (11)$$

Remark. Note that, the definition of TSW-SL_p depends on the space of sampled tree systems \mathbb{T} , the distribution σ on \mathbb{T} , and the splitting function α . For simplifying the notation, we omit them.

We use the Monte Carlo method to approximate the intractable expectation in Eq. (11) as follows:

$$\widehat{\text{TSW-SL}}_p(\mu, \nu) = \left(\frac{1}{L} \sum_{i=1}^L W_{d_{\mathcal{L}_i},p}^p(\mathcal{R}_{\mathcal{L}_i}^{\alpha}\mu, \mathcal{R}_{\mathcal{L}_i}^{\alpha}\nu) \right)^{\frac{1}{p}}, \quad (12)$$

where $\mathcal{L}_1, \dots, \mathcal{L}_L \stackrel{i.i.d.}{\sim} \sigma$ and are referred to as projecting tree systems. For $p \geq 1$, the TSW-SL_p distance is, indeed, a metric on $\mathcal{P}(\mathbb{R}^d)$. The proof for the below theorem is provided in Appendix C.1.

Theorem 5.2. For $p \geq 1$, the TSW-SL_p is a metric on $\mathcal{P}(\mathbb{R}^d)$.

Remark. If tree systems in \mathcal{T} have only one line, i.e. $n = 1$, then in Definition 4.1, the splitting α is the constant function 1, and the Radon Transform \mathcal{R}^{α} is the same as the usual Radon Transform, since projecting measures on a line only requires the direction of the line. Also, by the sampling process in Subsection 3.3, σ now is the distribution of direction θ_1 , which is $\mathcal{U}(\mathbb{S}^{d-1})$. In this case, TSW-SL_p in Eq. (11) is identical to SW_p in Eq. 2. Also, in Appendix D, we introduce *Max Tree-Sliced Wasserstein Distance on System of Lines* (MaxTSW-SL), which is an analog of MaxSW [6].

5.2 Discrete Measures and Closed-Form Expression

We now consider discrete measures to provide a concrete algorithm to compute our Tree-Sliced Distance variant. Let μ and ν be discrete measures in $\mathcal{P}(\mathbb{R}^d)$, and by projecting these measures on tree system \mathcal{L} in \mathbb{T} by $\mathcal{R}_{\mathcal{L}}^{\alpha}$, we get two discrete measures $\mathcal{R}_{\mathcal{L}}^{\alpha}\mu$ and $\mathcal{R}_{\mathcal{L}}^{\alpha}\nu$ on \mathcal{L} . Our goal is efficiently computing $\text{TSW-SL}_p(\mu, \nu)$ by the Monte Carlo estimation, which means computing the p -Wasserstein distance with ground tree metric:

$$W_{d_{\mathcal{L}_i},p}^p(\mathcal{R}_{\mathcal{L}_i}^{\alpha}\mu, \mathcal{R}_{\mathcal{L}_i}^{\alpha}\nu), \quad (13)$$

on L samples $\mathcal{L}_1, \dots, \mathcal{L}_L$. Unlike the one-dimensional $W_p^p(\theta_{\#}\mu, \theta_{\#}\nu)$ term of SW_p in Eq. (2) has the closed-form expression by cumulative distribution functions of $\theta_{\#}\mu, \theta_{\#}\nu$, the $W_{d_{\mathcal{L}_i},p}^p(\mathcal{R}_{\mathcal{L}_i}^{\alpha}\mu, \mathcal{R}_{\mathcal{L}_i}^{\alpha}\nu)$

does not always have closed-form expression. **It only has closed-form expression when $p = 1$** , provided by Eq. (4). We skip all related notations and simply write it as follows:

$$W_{d_{\mathcal{L}},1}(\mathcal{R}_{\mathcal{L}}^{\alpha}\mu, \mathcal{R}_{\mathcal{L}}^{\alpha}\nu) = \sum_{e \in \mathcal{T}} w_e \cdot \left| \mathcal{R}_{\mathcal{L}}^{\alpha}\mu(\Gamma(v_e)) - \mathcal{R}_{\mathcal{L}}^{\alpha}\nu(\Gamma(v_e)) \right|. \quad (14)$$

Algorithm. Assume that each measures μ and ν support on N and M points in \mathbb{R}^d , respectively. So the probability distribution functions of μ and ν are $\mu(x) = (1/N) \cdot \sum_{i=1}^N u_i \delta(x - a_i)$ and $\nu(x) = (1/M) \cdot \sum_{i=1}^M v_i \delta(x - b_i)$. For line l of tree system \mathcal{L} , denoted as $l = (x, \theta)$:

1. To project a_1 on (x, θ) , we compute $(a_1 - x) \cdot \theta$;
2. The mass of the projection of a_1 on (x, θ) is computed by $\alpha_l(a_1) \cdot u_1$.
3. Similar for other points of supports. Then sort the projections of supports on the line.

We get two discrete measures on $\mathcal{R}_{\mathcal{L}}^{\alpha}\mu$ and $\mathcal{R}_{\mathcal{L}}^{\alpha}\nu$ on \mathcal{L} by projecting supports and splitting mass, and also the actual tree (as graph) on \mathcal{L} by sorting (refer to A.12), then use Eq. (14) to compute $W_{d_{\mathcal{L}},1}(\mathcal{R}_{\mathcal{L}}^{\alpha}\mu, \mathcal{R}_{\mathcal{L}}^{\alpha}\nu)$. We summarize the computation by Algorithm 2.

Algorithm 2 Tree Sliced Wasserstein distance on System of Lines.

Input: Probability measures μ and ν , the number of lines in each tree system n , the number of tree systems L , a splitting function $\alpha: \mathbb{R}^d \rightarrow \Delta_n$.

Set $\widehat{\text{TSW-SL}}_1(\mu, \nu) = 0$.

for $i = 1$ to L **do**

Sampling tree system $\mathcal{L}_i = ((x_1^{(i)}, \theta_1^{(i)}), \dots, (x_n^{(i)}, \theta_n^{(i)}))$.

Projecting μ and ν onto \mathcal{L}_i to get $\mathcal{R}_{\mathcal{L}_i}^{\alpha}\mu$ and $\mathcal{R}_{\mathcal{L}_i}^{\alpha}\nu$.

Compute $\widehat{\text{TSW-SL}}_1(\mu, \nu) = \widehat{\text{TSW-SL}}_1(\mu, \nu) + (1/L) \cdot W_{d_{\mathcal{L}_i},1}(\mathcal{R}_{\mathcal{L}_i}^{\alpha}\mu, \mathcal{R}_{\mathcal{L}_i}^{\alpha}\nu)$.

end for

Return: $\widehat{\text{TSW-SL}}_1(\mu, \nu)$.

Time complexity. The time complexity of TSW-SL, like the SW, comes mostly from the support projecting and sorting. Assume $N \geq M$. Since it requires projecting on $L \times n$ lines and sorting N points on each line, so the time complexity for TSW-SL is $\mathcal{O}(LnN \log(N) + LndN)$. This is the same as SW, when the number of lines for projecting are equal. Consequently, in our experiments, we will compare TSW-SL to SW or some improved SW variants with the same number of lines.

Remark. For general $p \geq 1$, naively alternating the RHS of Eq. 14 will lead us to the Sobolev Transport in Eq. (5), and **it is not the same as $W_{d_{\mathcal{L}},p}$ unless $p = 1$** :

$$W_{d_{\mathcal{L}},p}(\mu, \nu) \neq \left(\sum_{e \in \mathcal{T}} w_e \cdot \left| \mu(\Gamma(v_e)) - \nu(\Gamma(v_e)) \right|^p \right)^{\frac{1}{p}} = \text{ST}_p(\mathcal{R}_{\mathcal{L}}^{\alpha}\mu, \mathcal{R}_{\mathcal{L}}^{\alpha}\nu), \quad \text{for } p > 1. \quad (15)$$

Nevertheless, since the ST_p itself is also a distance on measures supported on a tree (see [18], and the formula in Eq. (15) for all $p \geq 1$ can be computed the same as in Algorithm 2, so we use Eq. 15 for both cases $p = 1$ and $p > 1$ in our experiments.

Table 1: Average Wasserstein distance between source and target distributions of 10 runs on Swiss Roll and 25 Gaussians datasets. All methods use 100 projecting directions.

Methods	Swiss Roll						25 Gaussians					
	Step					Time/Iter(s)	Step					Time/Iter(s)
	500	1000	1500	2000	2500		500	1000	1500	2000	2500	
SW	<u>5.73e-3</u>	2.04e-3	1.23e-3	1.11e-3	1.05e-3	0.009	<u>1.61e-1</u>	9.52e-2	3.44e-2	2.56e-2	2.20e-2	0.006
MaxSW	2.47e-2	1.03e-2	6.10e-3	4.47e-3	3.45e-3	2.46	5.09e-1	2.36e-1	1.33e-1	9.70e-2	8.48e-2	2.38
SWGG	3.84e-2	1.53e-2	1.02e-2	4.49e-3	3.57e-5	0.011	3.10e-1	1.17e-1	3.38e-2	3.58e-3	2.54e-4	0.009
LCVSW	7.28e-3	1.40e-3	1.38e-3	1.38e-3	1.36e-3	0.010	3.38e-1	<u>6.64e-2</u>	3.06e-2	3.06e-2	3.02e-2	0.009
TSW-SL	9.41e-3	2.03e-7	9.63e-8	4.44e-8	3.65e-8	0.014	3.49e-1	9.06e-2	<u>2.96e-2</u>	<u>1.20e-2</u>	3.03e-7	0.010
MaxTSW-SL	2.75e-6	<u>8.24e-7</u>	<u>5.14e-7</u>	<u>5.02e-7</u>	<u>5.00e-7</u>	2.53	1.12e-1	8.28e-3	1.61e-6	7.32e-7	<u>5.19e-7</u>	2.49

6 Experimental Results

In this section, we present empirical results that illustrate the advantages of the TSW-SL distance relative to the traditional SW distance and its variants. Additionally, we demonstrate that MaxTSW-SL leverages the original MaxSW [6] through the optimization of the tree system, significantly enhancing the performance of MaxSW. We particularly emphasize the superior efficacy of our approach across three specific applications: gradient flows, image style transfer and generative models. Splitting function α will be initialized randomly or can be learned by a simple fully connected feedforward network, and the number of projecting directions will be the same across all baselines.

6.1 Gradient Flows

Setting We present our experimental results on gradient flows. More specifically, in gradient flows, we aim to minimize $\text{TSW-SL}(\mu, \nu)$, where μ and ν represent the source distribution and the target distribution by the iterative optimization process.

Baselines and Datasets We compare our proposed TSW-SL with 4 baselines: vanilla SW, MaxSW [6], SWGG [25] and LCVSW [32]. We use $L = 100$ in SW variants and $L = 25, n = 4$ in TSW-SL for a fair comparison. Detailed training settings are presented in Appendix E.1. We use Swiss Roll and 25 Gaussians datasets as in [14].

Results In Table 1, we present the performance and runtime of various methods on the Swiss Roll and 25 Gaussians datasets, focusing on the reduction of the Wasserstein distance over iterations. Across both datasets, our TSW-SL method demonstrates superior performance, significantly reducing the Wasserstein distance. Although the time per iteration for TSW-SL is slightly higher, the substantial reduction in Wasserstein distance underscores its efficiency across both datasets. It is also worth noting that our MaxTSW-SL method shows a significant decrease in the Wasserstein distance compared to MaxSW, highlighting its improved performance and effectiveness.

The details of datasets, training setup, and hyperparameters are provided in Appendix E.

Table 2: Average FID and IS score of 3 runs on CIFAR10 and CelebA.

	CIFAR10 (32x32)		CelebA (64x64)		CIFAR10 (32x32)		CelebA (64x64)
	FID(↓)	IS(↑)	FID(↓)		FID(↓)	IS(↑)	FID(↓)
SW ($L = 50$)	16.80 ± 0.45	7.97 ± 0.05	9.97 ± 1.02	SW ($L = 500$)	14.23 ± 0.84	8.25 ± 0.05	9.62 ± 0.42
TSW-SL ($L = 10, n = 5$)	15.44 ± 0.42	8.14 ± 0.05	9.63 ± 0.46	TSW-SL ($L = 100, n = 5$)	13.27 ± 0.23	8.30 ± 0.01	8.90 ± 0.49
TSW-SL ($L = 17, n = 3$)	15.9 ± 0.35	8.10 ± 0.04	8.98 ± 0.75	TSW-SL ($L = 167, n = 3$)	14.18 ± 0.38	8.28 ± 0.07	8.90 ± 0.38

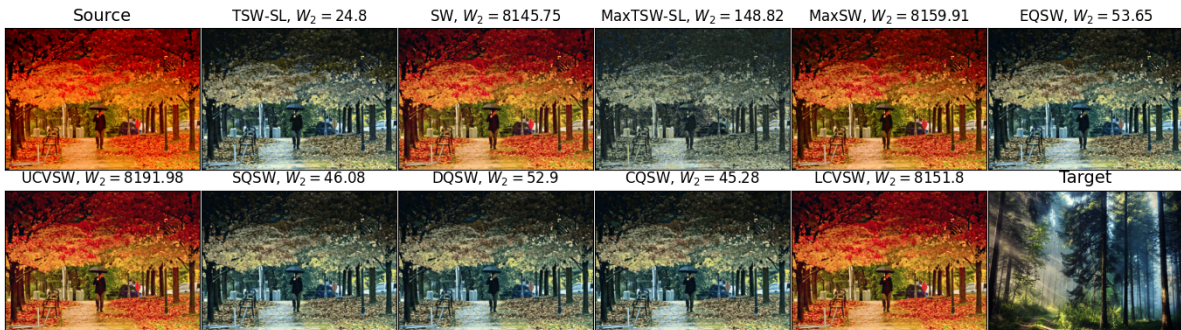


Figure 4: Style-transferred images from different models with 100 projecting directions.

6.2 Image Style Transfer

Setting Given a source image and a target image, we represent their respective color palettes as matrices X and Y , each with dimensions $n \times 3$ (where n denotes the number of pixels). We traverse along the curve connecting P_X and P_Y . However, owing to the color palette values (RGB) lying within the set $\{0, \dots, 255\}$, an additional rounding step is necessary during the final Euler iterations. Additionally, we increase the number of iterations to 1000 and utilize a larger step size of 1.

Baselines We assess the style-transferred images generated by SW [3], MaxSW [6], EQSW [29], UCVSW [32], SQSW [29], DQSW [29], CQSW [29], LCVSW [32] to compare with TSW-SL and MaxTSW-SL. We use $L = 100$ in SW variants and $L = 25, n = 4$ in TSW-SL for a fair comparison.

Results We present the Wasserstein distances at the final time step alongside the corresponding transferred images from SW, TSW-SL, MaxSW, MaxTSW-SL, EQSW, UCVSW, SQSW, DQSW, CQSW, and LCVSW in Figure 4. TSW-SL’s generated image notably shares the most common properties with the target image. This is evident from the smallest Wasserstein distance observed after the final step of our generated image, which represents that our method decreases Wasserstein distance significantly compared to SW and its variants using the same number of lines. We extend our evaluation to present the effectiveness of our MaxTSW-SL with the original MaxSW one by showing that our methods improve MaxSW notably measured by both qualitative and quantitative results.

6.3 Generative Models

Architecture To evaluate the effectiveness of our framework in generative tasks, we employ the SNGAN architecture [27]. In greater detail, our approach is based on the methodology of

the sliced Wasserstein generator [7], with details provided in the Appendix E.3. Specifically, we conduct deep generative modeling experiments on the CIFAR-10 dataset, which consists of images sized 32x32 [16], and on the non-cropped CelebA dataset, with images sized 64x64 [7].

In order to show the empirical advantage of our method in enhancing the ability of generative models, we utilize two primary metrics: the Fréchet Inception Distance (FID) score [11] and the Inception Score (IS) [44]. We do not report the IS for the CelebA dataset because it does not effectively capture the perceptual quality of face images [11].

Results We present the result of SW and TSW-SL methodologies on the CIFAR10 and CelebA datasets in Table 2, leveraging FID and IS as our metric. We use $L = 50$ in SW compared to $L = 10, n = 5$ and $L = 16, n = 3$ in TSW-SL, respectively. Same for 500 projecting directions.

Our findings reveal that TSW-SL markedly surpasses SW, elucidating a considerable performance differential. On the CIFAR10 dataset, with 50 projecting directions, TSW-SL achieves an 8% reduction in FID and a 2% enhancement in IS; and, with 500 directions, the FID reduction is 7%, accompanied by a marginal increase in IS. Similarly, on the CelebA dataset, TSW-SL demonstrates significant improvements. With 50 projecting directions, TSW-SL realizes a 10% reduction in FID compared to SW; and, with 500 directions, the FID improvement is 7.5%. These results underscore the superior efficacy of TSW-SL in generating more realistic and diverse images relative to SW, with the disparities in FID and IS highlighting the substantial qualitative advancements of the TSW-SL approach. We further provide quantitative results in Appendix E.3.

7 Conclusion

We propose the novel Tree-Sliced Wasserstein Distance on System of Lines (TSW-SL) which comes from our Radon Transform on System of Lines, a variant of the original Radon Transform. We verify key properties of the transform and also TSW-SL. Compared to previous work on SW variants, TSW-SL allows projecting measures onto larger geometrical meaningful spaces which are tree systems, instead of lines as in SW, meanwhile maintaining low computational cost. We empirically illustrate the advantages of TSW-SL across various application tasks such as gradient flows, image style transfer, and generative models. It is worth noting that our naive TSW-SL idea still has huge room for improvement, for instance, deeper studying in splitting function or leveraging techniques that can be used for improving SW. It can be considered as one limitation of our paper, and we leave it for future works.

Supplement to “Tree-Sliced Wasserstein Distance on a System of Lines”

Table of Contents

A Tree System	14
A.1 System of Lines	14
A.2 System of Lines with Tree Structures (Tree System)	15
A.3 Topological Properties of Tree Systems	16
A.4 Construction of Tree Systems	19
B Space of Integrable Functions on a System of Lines	21
B.1 Space of Lebesgue integrable functions on a system of lines	21
B.2 Space of probability distributions on a system of lines	23
C Theoretical Proofs for TSW-SL	23
C.1 Proof of Theorem 5.2	23
C.2 Proof of Theorem D.2	24
D Max Tree Sliced Wasserstein Distance on System of Lines.	25
E Experimental details	26
E.1 Gradient flows	26
E.2 Image style transfer	26
E.3 Generative models	27
E.4 Computational infrastructure	28
F Broader Impact	29

A Tree System

In this section, we will introduce the notion of a tree system, starting from a bunch of lines with no structure, and adding a tree structure to finally get a well-defined metric space with tree metric. Note that some statements in this section are slightly different from those in the paper, but the ideas are identical.

A.1 System of Lines

We have a definition of lines by parameterization. Observe that, a line in \mathbb{R}^d is completely determined by a pair $(x, \theta) \in \mathbb{R}^d \times \mathbb{S}^{d-1}$ via $x + t \cdot \theta, t \in \mathbb{R}$.

Definition A.1 (Line and System of lines in \mathbb{R}^d). A *line* in \mathbb{R}^d is an element (x, θ) of $\mathbb{R}^d \times \mathbb{S}^{d-1}$, and the *image* of a line (x, θ) is defined by:

$$\text{Im}(x, \theta) := \{x + t \cdot \theta : t \in \mathbb{R}\} \subset \mathbb{R}^d. \tag{16}$$

For $n \geq 1$, a *system of n lines* in \mathbb{R}^d is a sequence of n lines.

Remark. A line in \mathbb{R}^d is usually denoted, or indexed, by $l = (x_l, \theta_l) \in \mathbb{R}^d \times \mathbb{S}^{d-1}$. Here, x_l and θ_l are called *source* and *direction* of l , respectively. Denote $(\mathbb{R}^d \times \mathbb{S}^{d-1})^n$ by \mathbb{L}_n^d , which is the *collection of systems of n lines in \mathbb{R}^d* , and an element of \mathbb{L}_n^d is usually denoted by \mathcal{L} .

Definition A.2 (Ground Set). The *ground set* of a system of lines \mathcal{L} is defined by:

$$\bar{\mathcal{L}} := \left\{ (x, l) \in \mathbb{R}^d \times \mathcal{L} : x = x_l + t_x \cdot \theta_l \text{ for some } t_x \in \mathbb{R} \right\}.$$

For each element $(x, l) \in \bar{\mathcal{L}}$, we sometime write (x, l) as (t_x, l) , where $t_x \in \mathbb{R}$, which presents the parameterization of x on l by source x_l and direction θ_l , as $x = x_l + t_x \cdot \theta_l$.

Remark. In other words, the ground set $\bar{\mathcal{L}}$ is the disjoint union of images of lines in \mathcal{L} :

$$\bar{\mathcal{L}} = \bigsqcup_{l \in \mathcal{L}} \text{Im}(l).$$

This notation seems to be redundant, but will be helpful when we define the notion of functions on $\bar{\mathcal{L}}$.

A.2 System of Lines with Tree Structures (Tree System)

Consider a finite system of lines \mathcal{L} in \mathbb{R}^d . Assume that these lines are geometrically distinct, i.e. their images are distinct. Define the graph $\mathcal{G}_{\mathcal{L}}$ associated with \mathcal{L} , where \mathcal{L} is the set of nodes in $\mathcal{G}_{\mathcal{L}}$, and two nodes are adjacent if the two corresponding lines intersect each other. Here, saying two lines in \mathbb{R}^d intersect means their images have exactly one point in common.

Definition A.3 (Connected system of lines). \mathcal{L} is called *connected* if the associated graph $\mathcal{G}_{\mathcal{L}}$ is connected.

Remark. Intuitively, each edge of $\mathcal{G}_{\mathcal{L}}$ represents the intersection of its endpoints. If \mathcal{L} is connected, for every two points that each one lies on some lines in \mathcal{L} , one can travel to the other through lines in \mathcal{L} .

From now on, we will only consider the case \mathcal{L} is connected. Recall the notion of a spanning tree of a graph \mathcal{G} , which is a subgraph of \mathcal{G} that contains all nodes of \mathcal{G} , and also is a tree.

Definition A.4 (Tree system of lines). Let \mathcal{L} be a connected system of lines. A spanning tree \mathcal{T} of $\mathcal{G}_{\mathcal{L}}$ is called a *tree structure of \mathcal{L}* . A pair $(\mathcal{L}, \mathcal{T})$ consists of a connected system of lines \mathcal{L} and a tree structure \mathcal{T} of \mathcal{L} is called a *tree system of lines*.

Remark. For short, we usually call a tree system of lines as a *tree system*. In a tree system $(\mathcal{L}, \mathcal{T})$, images of two lines of \mathcal{L} can intersect each other even when they are not adjacent in \mathcal{T} .

Let r be an arbitrary line of \mathcal{L} . Denote \mathcal{T}_r as the tree \mathcal{T} rooted at r , and denote the (rooted) tree system as $(\mathcal{L}, \mathcal{T}_r)$ if we want to specify the root.

Definition A.5 (Depth of lines in a tree system). Let $(\mathcal{L}, \mathcal{T}_r)$ be a tree system. For each $m \geq 0$, a line $l \in \mathcal{L}$ is called a *line of depth m* if the (unique) path from r to l in \mathcal{T} has length m . Denote \mathcal{L}_m as the *set of lines of depth m* .

Remark. Note that $\mathcal{L}_0 = \{r\}$. Let T be the maximum length of paths in \mathcal{T} start from r , which is called the *depth of the line system*. \mathcal{L} has a partition as $\mathcal{L} = \mathcal{L}_0 \sqcup \mathcal{L}_1 \sqcup \dots \sqcup \mathcal{L}_T$.

For $l \in \mathcal{L}$ that is not the root, denote $\text{pr}(l) \in \mathcal{L}$ as the *parent of l* , i.e. the (unique) node on the unique path from l to r that is adjacent to l . Note that, by definition, l and $\text{pr}(l)$ intersect each other. We sometimes omit the root when the context is clear.

Definition A.6 (Canonical tree system). A tree system $(\mathcal{L}, \mathcal{T})$ is called a *canonical tree system* if for all $l \in \mathcal{L}$ that is not the root, the intersection of l and $\text{pr}(l)$ is the source x_l of l .

Remark. In other words, in a canonical tree system, a line that differs from the root will have its source lies on its parent. For the rest of the paper, a tree system $(\mathcal{L}, \mathcal{T})$ will be considered to be a canonical tree system.

A.3 Topological Properties of Tree Systems

We will introduce the notion of the topological space of a tree system. Let $(\mathcal{L}, \mathcal{T})$ be a (canonical) tree system. Consider a graph where the nodes are elements of $\bar{\mathcal{L}}$; (x, l) and (x', l') are adjacent if and only if one of the following conditions holds:

1. $l = \text{pr}(l')$, $x = x'$, and x' is the source of l' .
2. $l' = \text{pr}(l)$, $x = x'$, and x is the source of l .

Let \sim be the relation on $\bar{\mathcal{L}}$ such that $(x, l) \sim (x', l')$ if and only if (x, l) and (x', l') are connected in the above graph. By design, \sim is an equivalence relation on $\bar{\mathcal{L}}$. The set of all equivalence classes in $\bar{\mathcal{L}}$ with respect to the equivalence relation \sim as $\Omega_{\mathcal{L}} = \bar{\mathcal{L}} / \sim$.

Remark. In other words, we identify the source of lines to the corresponding point on its parent.

We recall the notion of disjoint union topology and quotient topology in [9]. For a line l in \mathbb{R}^d , the image $\text{Im}(l)$ is a topological space, moreover, a metric space, that is homeomorphic and isometric to \mathbb{R} via the map $t \mapsto x_l + t \cdot \theta_l$. The metric on $\text{Im}(l)$ is $d_l(x, x') = |t_x - t_{x'}|$ for all $x, x' \in \text{Im}(l)$. For each $l \in \mathcal{L}$, consider the injection map:

$$\begin{aligned} f_l : \text{Im}(l) &\longrightarrow \bigsqcup_{l \in \mathcal{L}} \text{Im}(l) = \bar{\mathcal{L}} \\ x &\longmapsto (x, l). \end{aligned}$$

$\bar{\mathcal{L}} = \bigsqcup_{l \in \mathcal{L}} \text{Im}(l)$ now becomes a topological space with the disjoint union topology, i.e. the finest topology on $\bar{\mathcal{L}}$ such that the map f_l is continuous for all $l \in \mathcal{L}$. Also, consider the quotient map:

$$\begin{aligned} \pi : \bar{\mathcal{L}} &\longrightarrow \Omega_{\mathcal{L}} \\ (x, l) &\longmapsto [(x, l)]. \end{aligned}$$

$\Omega_{\mathcal{L}}$ now becomes a topological space with the quotient topology, i.e. the finest topology on $\Omega_{\mathcal{L}}$ such that the map π is continuous.

Definition A.7 (Topological space of a tree system). The topological space $\Omega_{\mathcal{L}}$ is called the *topological space of a tree system* $(\mathcal{L}, \mathcal{T})$.

Remark. In other words, $\Omega_{\mathcal{L}}$ is formed by gluing all images $\text{Im}(l)$ along the relation \sim .

We show that the topological space $\Omega_{\mathcal{L}}$ is metrizable.

Definition A.8 (Paths in $\Omega_{\mathcal{L}}$). For a and b in $\Omega_{\mathcal{L}}$ with $a \neq b$, a *path from a to b in $\Omega_{\mathcal{L}}$* is a continuous injective map $\gamma: [0, 1] \rightarrow \Omega_{\mathcal{L}}$ where $\gamma(0) = a$ and $\gamma(1) = b$. By convention, for a in $\Omega_{\mathcal{L}}$, the path from a to a in $\Omega_{\mathcal{L}}$ is the constant map $\gamma: [0, 1] \rightarrow \Omega_{\mathcal{L}}$ such that $\gamma(t) = a$ for all $t \in [0, 1]$. For a path γ from a to b , the *image of γ* is defined by:

$$\text{Im}(\gamma) := \gamma([0, 1]) \subset \Omega_{\mathcal{L}}. \quad (17)$$

Theorem A.9 (Existence and uniqueness of path in $\Omega_{\mathcal{L}}$). *For all a and b in $\Omega_{\mathcal{L}}$, there exist a path γ from a to b in $\Omega_{\mathcal{L}}$. Moreover, γ is unique up to a re-parameterization, i.e. if γ and γ' are two path γ from a to b in $\Omega_{\mathcal{L}}$, there exist a homeomorphism $\varphi: [0, 1] \rightarrow [0, 1]$ such that $\gamma = \gamma' \circ \varphi$.*

Proof. All previous results we state in this proof can be found in [28, 42, 9]. For two point a, b on the real line \mathbb{R} , all paths from a to b are homotopic to each other. In other words, all paths from a to b are homotopic to the canonical path:

$$\begin{aligned} \gamma_{a,b} : [0, 1] &\longrightarrow \mathbb{R} \\ t &\longmapsto (1-t) \cdot a + t \cdot b. \end{aligned}$$

Now consider two point a, b on space $\Omega_{\mathcal{L}}$. Observe that $\Omega_{\mathcal{L}}$ is path-connected by design and by the fact that \mathbb{R} is path-connected. Consider a curve from a to b on $\Omega_{\mathcal{L}}$, i.e. a continuous map $f: [0, 1] \rightarrow \Omega_{\mathcal{L}}$, and consider the set consists of sources of lines in \mathcal{L} that lie on the curve f , i.e. all the sources that belong to $f([0, 1])$. We choose the curve f that has the smallest set of sources. By the tree structure added to \mathcal{L} , all curves from a to b have the set of sources that contains the set of sources of f . We denote the sources belong to this set of f as s_1, \dots, s_{k-1} , and defined:

$$x_i = \inf f^{-1}(s_i) \text{ for all } 1 \leq i \leq k-1.$$

We reindex s_i such that:

$$x_1 \leq \dots \leq x_{k-1}$$

For convention, we define $s_0 = a$ and $s_k = b$. By design, for $i = 0, \dots, k-1$, we have s_i and s_{i+1} line on the same line in \mathcal{L} . So by the result of paths on \mathbb{R} , there exist a path γ_i from s_i to s_{i+1} on $\Omega_{\mathcal{L}}$. Gluing $\gamma_0, \gamma_1, \dots, \gamma_{k-1}$ to get a path γ from $s_0 = a$ to $s_k = b$ on $\Omega_{\mathcal{L}}$ by:

$$\begin{aligned} \gamma : [0, 1] &\longrightarrow \Omega_{\mathcal{L}} \\ t &\longmapsto \gamma_i(k \cdot t - i) \text{ if } t \in \left[\frac{i}{k}, \frac{i+1}{k} \right], i = 0, \dots, k-1. \end{aligned}$$

It is clear to check γ is a path from a to b on Ω , and the uniqueness (up to re-parameterization) of γ comes from homotopy of paths in \mathbb{R} . \square

Remark. The image of a path from a to b does not depend on the chosen path γ by the uniqueness property. Indeed, for a homeomorphism $\varphi: [0, 1] \rightarrow [0, 1]$, we have $\gamma([0, 1]) = \gamma \circ \varphi([0, 1])$. Denote the image of *any path* from a to b by $P_{a,b}$.

Let μ be the standard Borel measure on \mathbb{R} , i.e. $\mu((a, b]) = b - a$ for every half-open interval $(a, b]$ in \mathbb{R} . For $l \in \mathcal{L}$, denote μ_l as the pushforward of μ by the map $t \mapsto x_l + t \cdot \theta_l$, which is a Borel measure on $\text{Im}(l)$. Denote the σ -algebra of Borel sets in $\bar{\mathcal{L}}$ and $\Omega_{\mathcal{L}}$ as $\mathcal{B}(\bar{\mathcal{L}})$ and $\mathcal{B}(\Omega_{\mathcal{L}})$, respectively.

Definition A.10 (Borel measure on $\bar{\mathcal{L}}$ and $\Omega_{\mathcal{L}}$). The map $\mu_{\bar{\mathcal{L}}}: \mathcal{B}(\Omega_{\mathcal{L}}) \rightarrow [0, \infty)$ that is defined by:

$$\mu_{\bar{\mathcal{L}}}(B) := \sum_{l \in \mathcal{L}} \mu_l(f_l^{-1}(B)) \quad , \quad \forall B \in \mathcal{B}(\bar{\mathcal{L}}),$$

is called the *Borel measure on $\bar{\mathcal{L}}$* . Define the *Borel measure on $\Omega_{\mathcal{L}}$* , denoted by $\mu_{\Omega_{\mathcal{L}}}$, as the pushforward of $\mu_{\bar{\mathcal{L}}}$ by the map $\pi: \bar{\mathcal{L}} \rightarrow \Omega_{\mathcal{L}}$.

It is straightforward to show that $\mu_{\bar{\mathcal{L}}}$ is well-defined, and indeed a Borel measure of $\bar{\mathcal{L}}$. As a corollary, $\mu_{\Omega_{\mathcal{L}}}$ is also a Borel measure of $\Omega_{\mathcal{L}}$.

Remark. By abuse of notation, we sometimes simply denote both of $\mu_{\bar{\mathcal{L}}}$ and $\mu_{\Omega_{\mathcal{L}}}$ as $\mu_{\mathcal{L}}$.

Theorem A.11 ($\Omega_{\mathcal{L}}$ is metrizable by a tree metric). Define the map $d_{\Omega}: \Omega_{\mathcal{L}} \times \Omega_{\mathcal{L}} \rightarrow [0, \infty)$ by:

$$d_{\mathcal{L}}(a, b) := \mu_{\mathcal{L}}(P_{a,b}) \quad , \quad \forall a, b \in \Omega_{\mathcal{L}}. \quad (18)$$

Then $d_{\mathcal{L}}$ is a metric on $\Omega_{\mathcal{L}}$, which makes $(\Omega_{\mathcal{L}}, d_{\mathcal{L}})$ a metric space. Moreover, $d_{\mathcal{L}}$ is a tree metric, and the topology on $\Omega_{\mathcal{L}}$ induced by $d_{\mathcal{L}}$ is identical to the topology of $\Omega_{\mathcal{L}}$.

Proof. It is straightforward to check that $d_{\mathcal{L}}$ is positive definite and symmetry. We show the triangle inequality holds for $d_{\mathcal{L}}$. Let a, b, c be points of $\Omega_{\mathcal{L}}$. It is enough to show that $P_{a,c}$ is a subset of $P_{a,b} \cup P_{b,c}$. Let γ_0, γ_1 be paths on Ω from a to b and from b to c , respectively. Consider the curve from a to c on Ω defined by:

$$\begin{aligned} \gamma : [0, 1] &\longrightarrow \Omega_{\mathcal{L}} \\ t &\longmapsto \gamma_i(2 \cdot t - i) \quad \text{if } t \in \left[\frac{i}{2}, \frac{i+1}{2} \right], i = 0, 1. \end{aligned}$$

It is clear that γ is a curve from a to c . We have $\gamma([0, 1])$ is exactly the union of $P_{a,b}$ and $P_{b,c}$. As in the proof of Theorem A.9, the set of sources of γ contains the set of sources lying on the path from a to c . So $\gamma([0, 1])$ contains $P_{a,c}$. \square

We have the below corollary says that: If we take finite points on $\Omega_{\mathcal{L}}$, together with the sources of lines, it induces a tree (as a graph) with nodes are these points; Moreover, we have a tree metric on this tree which is $d_{\mathcal{L}}$.

Corollary A.12. Let y_1, y_2, \dots, y_m be points on $\Omega_{\mathcal{L}}$. Consider the graph, where $\{y_1, \dots, y_m\} \cup \{x_l : l \in \mathcal{L}\}$ is the node set, and two nodes are adjacent if the (unique) path between this two nodes on $\Omega_{\mathcal{L}}$ does not contain any node, except them. Then this graph is a rooted tree at x_r , with an induced tree metric from $d_{\mathcal{L}}$.

A.4 Construction of Tree Systems

We present a way to construct a tree system in \mathbb{R}^d . First, we have a way to describe the structure of a rooted tree by a sequence of vectors.

Definition A.13 (Tree representation). Let T be a nonnegative integer, and n_1, \dots, n_T be T positive integer. A sequence $s = \{x_i\}_{i=0}^T$, where x_i is a vector of n_i nonnegative numbers, is called a *tree representation* if $x_0 = [1]$, and for all $1 \leq i \leq T$, n_i is equal to the sum of all entries in vector x_{i-1} .

Example A.14. For $T = 5$ and $\{n_i\}_{i=0}^5 = \{1, 3, 4, 2, 3\}$, the sequence:

$$s : [1] \rightarrow [3] \rightarrow [2, 1, 1] \rightarrow [1, 0, 2, 0] \rightarrow [1, 2], [0, 0, 1]$$

is a tree representation.

For a tree representation $s = \{x_i\}_{i=0}^T$, a *tree system of type s* is a tree system that is inductively constructed step-by-step as follows:

- Step 0. Sample a point $x_r \in \mathbb{R}^d$ and a direction $\theta_r \in \mathbb{S}^{d-1}$. Define r as the line that passes through x_r with direction θ_r . We call r as the line of depth 0.
- Step i. On the j -th line of depth $i - 1$, sample $(x_i)_j$ points where $(x_i)_j$ is the j -th entry of vector x_i . For each of these points, denoted as x_l , sample a direction $\theta_l \in \mathbb{S}^{d-1}$, and define l is the line that passes through x_l with direction θ_l . We call the set of all lines sampled at this step as the set of lines of depth i , and order them by the order that they are sampled.

By this construction, we will get a system of lines \mathcal{L} in \mathbb{R}^d , together with a tree structure \mathcal{T}_r . The pair $(\mathcal{L}, \mathcal{T}_r)$ forms a tree system, which is canonical by design, and is said to be of type s . Denote \mathbb{T}_s as the *set of all tree systems of type s* .

Remark. A tree system in of type s has $n = \sum_{i=0}^T \sum_{j=1}^{n_i} (x_i)_j$ lines. Observe that constructing a tree system of type s only depends on sampling n points and n directions, so by some assumptions on the probability distribution of these points and directions, we will have a probability distribution on \mathbb{T}_s . Note that:

1. x_r is sampled from a distribution on \mathbb{R}^d ;
2. For all $l \neq r$, x_l is sampled from a distribution on \mathbb{R} ;
3. For all l , θ_l is sampled from a distribution on \mathbb{S}^{d-1} .

We have some examples of tree presentations s and distribution on \mathbb{T}_s .

Example A.15 (Lines pass through origin). Consider the tree representation s :

$$s : [1], \tag{19}$$

and the distributions on \mathbb{T}_s is determined by:

1. $x_r = 0 \in \mathbb{R}^d$;
2. $\theta_r \sim \mathcal{U}(\mathbb{S}^{d-1})$.

In this case, \mathbb{T}_s is identical to the set of lines that pass through the origin 0.

Example A.16 (Concurrent lines). Consider the tree representation s :

$$s : [1] \rightarrow [n-1], \quad (20)$$

and the distributions on \mathbb{T}_s is determined by:

1. $x_r \sim \mu_r$ for an $\mu_r \in \mathcal{P}(\mathbb{R}^d)$;
2. For all $l \neq r$, $x_l = x_r$;
3. For all l , $\theta_l \sim \mathcal{U}(\mathbb{S}^{d-1})$;
4. x_r and all θ_l 's are pairwise independent.

In this case, \mathbb{T}_s is identical to the set of all tuples of n concurrent lines.

Example A.17 (Series of lines). Consider the tree representation s :

$$s : [1] \rightarrow [1] \rightarrow \dots \rightarrow [1], \quad (21)$$

and the distributions on \mathbb{T}_s is determined by:

1. $x_r \sim \mu_r$ for an $\mu_r \in \mathcal{P}(\mathbb{R}^d)$;
2. For all $l \neq r$, $x_l \sim \mu_l$ for an $\mu_l \in \mathcal{P}(\mathbb{R})$;
3. For all l , $\theta_l \sim \mathcal{U}(\mathbb{S}^{d-1})$;
4. All x_l 's and all θ_l 's are pairwise independent.

In this case, we call \mathbb{T}_s as the set of all series of n lines. This is the same as the sampling process in Subsection 3.3 and Algorithm 1.

Example A.18. For an arbitrary tree representation s , the distributions on \mathbb{T}_s is determined by:

1. x_r is sampled from the uniform distribution on a bounded subset of \mathbb{R}^d , for instance, $\mu_r \sim \mathcal{U}([0, 1]^d)$;
2. For $l \neq r$, x_l will be sampled from the uniform distribution on a bounded subset of \mathbb{R} , for instance, $\mu_l \sim \mathcal{U}([0, 1])$;
3. For all l , θ_l will be sampled from the uniform distribution on \mathbb{S}^{d-1} , i.e $\theta_l \sim \mathcal{U}(\mathbb{S}^{d-1})$;
4. Together with assumptions on independence between all x_r 's and all θ_l 's.

B Space of Integrable Functions on a System of Lines

We introduce the notions of the space of Lebesgue integrable functions and the space of probability distributions on a system of lines. Let \mathcal{L} be a system of n lines.

B.1 Space of Lebesgue integrable functions on a system of lines

Denote $L^1(\mathbb{R}^d)$ as the space of Lebesgue integrable functions on \mathbb{R}^d with norm $\|\cdot\|_1$:

$$L^1(\mathbb{R}^d) = \left\{ f: \mathbb{R}^d \rightarrow \mathbb{R} : \|f\|_1 = \int_{\mathbb{R}^d} |f(x)| dx < \infty \right\}. \quad (22)$$

As usual, two functions $f_1, f_2 \in L^1(\mathbb{R}^d)$ are considered to be identical if $f_1(x) = f_2(x)$ for almost everywhere on \mathbb{R}^d .

Definition B.1 (Lebesgue integrable function on a system of lines). A *Lebesgue integrable function on \mathcal{L}* is a function $f: \bar{\mathcal{L}} \rightarrow \mathbb{R}$ such that:

$$\|f\|_{\mathcal{L}} := \sum_{l \in \mathcal{L}} \int_{\mathbb{R}} |f(t_x, l)| dt_x < \infty. \quad (23)$$

The *space of Lebesgue integrable functions on \mathcal{L}* is denoted by:

$$L^1(\mathcal{L}) := \left\{ f: \bar{\mathcal{L}} \rightarrow \mathbb{R} : \|f\|_{\mathcal{L}} = \sum_{l \in \mathcal{L}} \int_{\mathbb{R}} |f(t_x, l)| dt_x < \infty \right\}. \quad (24)$$

Remark. As an analog of integrable functions on \mathbb{R}^d , two functions $f_1, f_2 \in L^1(\mathcal{L})$ are considered to be identical if $f_1(x) = f_2(x)$ for almost everywhere on $\bar{\mathcal{L}}$. The space $L^1(\mathcal{L})$ with norm $\|\cdot\|_{\mathcal{L}}$ is a Banach space.

Recall that \mathcal{L} has n lines, we denote the $(n-1)$ -dimensional standard simplex as $\Delta_{n-1} = \{(a_i)_{i \in \mathcal{L}} : \sum_{i \in \mathcal{L}} a_i = 1\} \subset \mathbb{R}^n$. Let $\mathcal{C}(\mathbb{R}^d, \Delta_{n-1})$ be the space of continuous function from \mathbb{R}^d to $\Delta_{\mathcal{L}}$. Let \mathcal{L} be a system of lines in \mathbb{L}_n^d , α be a function in $\mathcal{C}(\mathbb{R}^d, \Delta_{n-1})$, we define an operator associated to α that transforms a Lebesgue integrable functions on \mathbb{R}^d to a Lebesgue integrable functions on \mathcal{L} . For $f \in \mathcal{P}(\mathbb{R}^d)$, define:

$$\begin{aligned} \mathcal{R}_{\mathcal{L}}^{\alpha} f : \bar{\mathcal{L}} &\longrightarrow \mathbb{R} \\ (x, l) &\longmapsto \int_{\mathbb{R}^d} f(y) \cdot \alpha(y)_l \cdot \delta(t_x - \langle y - x_l, \theta_l \rangle) dy, \end{aligned}$$

where δ is the 1-dimensional Dirac delta function.

Theorem B.2. For $f \in L^1(\mathbb{R}^d)$, we have $\mathcal{R}_{\mathcal{L}}^{\alpha} f \in L^1(\mathcal{L})$. Moreover, we have $\|\mathcal{R}_{\mathcal{L}}^{\alpha} f\|_{\mathcal{L}} \leq \|f\|_1$. In other words, the operator:

$$\mathcal{R}_{\mathcal{L}}^{\alpha}: L^1(\mathbb{R}^d) \rightarrow L^1(\mathcal{L}), \quad (25)$$

is well-defined, and is a linear operator.

Proof. Let $f \in L^1(\mathbb{R}^d)$. We show that $\|\mathcal{R}_{\mathcal{L}}^\alpha f\|_{\mathcal{L}} \leq \|f\|_1$. Indeed,

$$\|\mathcal{R}_{\mathcal{L}}^\alpha f\|_{\mathcal{L}} = \sum_{l \in \mathcal{L}} \int_{\mathbb{R}} |\mathcal{R}_{\mathcal{L}}^\alpha f(t_x, l)| dt_x \quad (26)$$

$$= \sum_{l \in \mathcal{L}} \int_{\mathbb{R}} \left| \int_{\mathbb{R}^d} f(y) \cdot \alpha(y)_l \cdot \delta(t_x - \langle y - x_l, \theta_l \rangle) dy \right| dt_x \quad (27)$$

$$\leq \sum_{l \in \mathcal{L}} \int_{\mathbb{R}^d} \left(\int_{\mathbb{R}} |f(y)| \cdot \alpha(y)_l \cdot \delta(t_x - \langle y - x_l, \theta_l \rangle) \cdot dt_x \right) dy \quad (28)$$

$$= \sum_{l \in \mathcal{L}} \int_{\mathbb{R}^d} |f(y)| \cdot \alpha(y)_l \cdot \left(\int_{\mathbb{R}} \delta(t_x - \langle y - x_l, \theta_l \rangle) dt_x \right) dy \quad (29)$$

$$= \sum_{l \in \mathcal{L}} \int_{\mathbb{R}^d} |f(y)| \cdot \alpha(y)_l dy \quad (30)$$

$$= \int_{\mathbb{R}^d} |f(y)| \cdot \sum_{l \in \mathcal{L}} \alpha(y)_l dy \quad (31)$$

$$= \int_{\mathbb{R}^d} |f(y)| dy \quad (32)$$

$$= \|f\|_1 < \infty. \quad (33)$$

So the operator $\mathcal{R}_{\mathcal{L}}^\alpha$ is well-defined, and is clearly a linear operator. \square

Definition B.3 (Radon transform on system of lines). For $\alpha \in \mathcal{C}(\mathbb{R}^d, \Delta_{n-1})$, the operator \mathcal{R}^α :

$$\begin{aligned} \mathcal{R}^\alpha : L^1(\mathbb{R}^d) &\longrightarrow \prod_{\mathcal{L} \in \mathbb{L}_n^d} L^1(\mathcal{L}) \\ f &\longmapsto (\mathcal{R}_{\mathcal{L}}^\alpha f)_{\mathcal{L} \in \mathbb{L}_n^d}. \end{aligned}$$

is called the *Radon transform on a system of lines*.

Many variants of Radon transform require the transforms to be injective. We show that the injectivity holds in the Radon transform on a system of lines.

Theorem B.4. \mathcal{R}^α is injective.

Proof. Since \mathcal{R}^α is linear, we show that if $\mathcal{R}^\alpha f = 0$, then $f = 0$. Let $f \in L^1(\mathbb{R}^d)$ such that $\mathcal{R}^\alpha f = 0$, which means $\mathcal{R}_{\mathcal{L}}^\alpha f = 0$ for all $\mathcal{L} \in \mathbb{L}_n^d$. Fix a line index l , consider the operator:

$$\int_{\mathbb{R}^d} f(y) \cdot \alpha(y)_l \cdot \delta(t_x - \langle y - x_l, \theta_l \rangle) dy = 0, \quad \forall t_x \in \mathbb{R}, (x_l, \theta_l) \in \mathbb{R}^d \times \mathbb{S}^{d-1}. \quad (34)$$

Note that for index l , $f(y) \cdot \alpha(y)_l$ is a function of y . Let x_l be fixed and θ_l varies in \mathbb{R}^d . By the injectivity of the usual Radon transform [10], we have $f(x) \cdot \alpha(x)_l = 0$ for all $x \in \mathbb{R}^d$. This holds for all line index l , so $f(x) = \sum_l f(x) \cdot \alpha(x)_l = 0$. So \mathcal{R}^α is injective. \square

Remark. By the proof, we can show a stronger result as follows: Let \mathbb{A} be a subset of \mathbb{L}_n^d such that for every index l and $\theta \in \mathbb{S}^{d-1}$, there exists $\mathcal{L} \in \mathbb{A}$ such that $\theta_l = \theta$, where θ_l is the direction of line with index l in \mathcal{L} . Roughly speaking, the set of directions in \mathcal{L} is $(\mathbb{S}^{d-1})^n$.

B.2 Space of probability distributions on a system of lines

Denote $\mathcal{P}(\mathbb{R}^d)$ as the space of all probability distribution on \mathbb{R}^d :

$$\mathcal{P}(\mathbb{R}^d) = \left\{ f: \mathbb{R}^d \rightarrow [0, \infty) : \|f\|_1 = 1 \right\} \subset L^1(\mathbb{R}^d).$$

Definition B.5 (Probability distribution on a system of lines). Let \mathcal{L} be a system of lines. A *probability distribution on \mathcal{L}* is a function $f \in L^1(\mathcal{L})$ such that $f: \bar{\mathcal{L}} \rightarrow [0, \infty)$ and $\|f\|_{\mathcal{L}} = 1$. The *space of probability distribution on \mathcal{L}* is defined by:

$$\mathcal{P}(\mathcal{L}) := \left\{ f: \bar{\mathcal{L}} \rightarrow [0, \infty) : \|f\|_{\mathcal{L}} = 1 \right\} \subset L^1(\mathcal{L}). \quad (35)$$

Corollary B.6. For $f \in \mathcal{P}^1(\mathbb{R}^d)$, we have $\mathcal{R}_{\mathcal{L}}^{\alpha} f \in \mathcal{P}(\mathcal{L})$. In other words, the restricted of Radon transform:

$$\mathcal{R}_{\mathcal{L}}^{\alpha}: \mathcal{P}(\mathbb{R}^d) \rightarrow \mathcal{P}(\mathcal{L}), \quad (36)$$

is well-defined.

Proof. Let $f \in \mathcal{P}^1(\mathbb{R}^d)$. It is clear that $\mathcal{R}_{\mathcal{L}}^{\alpha} f: \bar{\mathcal{L}} \rightarrow [0, \infty)$. We show that $\|\mathcal{R}_{\mathcal{L}}^{\alpha} f\|_{\mathcal{L}} = 1$. Indeed,

$$\|\mathcal{R}_{\mathcal{L}}^{\alpha} f\|_{\mathcal{L}} = \sum_{l \in \mathcal{L}} \int_{\mathbb{R}} \mathcal{R}_{\mathcal{L}}^{\alpha} f(t_x, l) dt_x \quad (37)$$

$$= \sum_{l \in \mathcal{L}} \int_{\mathbb{R}} \left(\int_{\mathbb{R}^d} f(y) \cdot \alpha(y)_l \cdot \delta(t_x - \langle y - x_l, \theta_l \rangle) dy \right) dt_x \quad (38)$$

$$= \int_{\mathbb{R}^d} f(y) dy = 1. \quad (39)$$

So $\mathcal{R}_{\mathcal{L}}^{\alpha} f \in \mathcal{P}(\mathcal{L})$, and $\mathcal{R}_{\mathcal{L}}^{\alpha}$ is well-defined. \square

C Theoretical Proofs for TSW-SL

We will omit almost-surely related conditions in the proofs, since it is clear to verify, and including them makes the proofs to be over-complicated.

C.1 Proof of Theorem 5.2

Proof. We want to show for $p \geq 1$:

$$\text{TSW-SL}_p(\mu, \nu) = \left(\mathbb{E}_{\mathcal{L} \sim \sigma} \left[W_{d_{\mathcal{L}}, p}^p(\mathcal{R}_{\mathcal{L}}^{\alpha} \mu, \mathcal{R}_{\mathcal{L}}^{\alpha} \nu) \right] \right)^{\frac{1}{p}}, \quad (40)$$

is a metric on $\mathcal{P}(\mathbb{R}^d)$.

Positive definiteness. For $\mu, \nu \in \mathcal{P}(\mathbb{R}^n)$, it is clear that $\text{TSW-SL}_p(\mu, \mu) = 0$ and $\text{TSW-SL}_p(\mu, \nu) \geq 0$. If $\text{TSW-SL}_p(\mu, \nu) = 0$, then $W_{d_{\mathcal{L}}, p}^p(\mathcal{R}_{\mathcal{L}}^{\alpha} \mu, \mathcal{R}_{\mathcal{L}}^{\alpha} \nu) = 0$ for all $\mathcal{L} \in \mathbb{T}$. Since $W_{d_{\mathcal{L}}, p}$ is a metric, we have $\mathcal{R}_{\mathcal{L}}^{\alpha} \mu = \mathcal{R}_{\mathcal{L}}^{\alpha} \nu$ for all $\mathcal{L} \in \mathbb{T}$. But \mathbb{T} is a subset of \mathbb{L}_n^d that satisfies the condition in the remark under the proof of Theorem B.4, so we have $\mu = \nu$.

Symmetry. For $\mu, \nu \in \mathcal{P}(\mathbb{R}^n)$, we have:

$$\text{TSW-SL}_p^p(\mu, \nu) = \mathbb{E}_{\mathcal{L} \sim \sigma} \left[W_{d_{\mathcal{L}, p}}^p(\mathcal{R}_{\mathcal{L}}^\alpha \mu, \mathcal{R}_{\mathcal{L}}^\alpha \nu) \right] \quad (41)$$

$$= \mathbb{E}_{\mathcal{L} \sim \sigma} \left[W_{d_{\mathcal{L}, p}}^p(\mathcal{R}_{\mathcal{L}}^\alpha \nu, \mathcal{R}_{\mathcal{L}}^\alpha \mu) \right] \quad (42)$$

$$= \text{TSW-SL}_p^p(\nu, \mu). \quad (43)$$

So $\text{TSW-SL}_p(\mu, \nu) = \text{TSW-SL}_p(\nu, \mu)$.

Triangle inequality. For $\mu_1, \mu_2, \mu_3 \in \mathcal{P}(\mathbb{R}^n)$, we have:

$$\text{TSW-SL}_p(\mu_1, \mu_2) + \text{TSW-SL}_p(\mu_2, \mu_3) \quad (44)$$

$$= \left(\mathbb{E}_{\mathcal{L} \sim \sigma} \left[W_{d_{\mathcal{L}, p}}^p(\mathcal{R}_{\mathcal{L}}^\alpha \mu_1, \mathcal{R}_{\mathcal{L}}^\alpha \mu_2) \right] \right)^{\frac{1}{p}} + \left(\mathbb{E}_{\mathcal{L} \sim \sigma} \left[W_{d_{\mathcal{L}, p}}^p(\mathcal{R}_{\mathcal{L}}^\alpha \mu_2, \mathcal{R}_{\mathcal{L}}^\alpha \mu_3) \right] \right)^{\frac{1}{p}} \quad (45)$$

$$\geq \left(\mathbb{E}_{\mathcal{L} \sim \sigma} \left[\left(W_{d_{\mathcal{L}, p}}(\mathcal{R}_{\mathcal{L}}^\alpha \mu_1, \mathcal{R}_{\mathcal{L}}^\alpha \mu_2) + W_{d_{\mathcal{L}, p}}(\mathcal{R}_{\mathcal{L}}^\alpha \mu_2, \mathcal{R}_{\mathcal{L}}^\alpha \mu_3) \right)^p \right] \right)^{\frac{1}{p}} \quad (46)$$

$$\geq \left(\mathbb{E}_{\mathcal{L} \sim \sigma} \left[W_{d_{\mathcal{L}, p}}^p(\mathcal{R}_{\mathcal{L}}^\alpha \mu_1, \mathcal{R}_{\mathcal{L}}^\alpha \mu_3) \right] \right)^{\frac{1}{p}} \quad (47)$$

$$= \text{TSW-SL}_p(\mu_1, \mu_3). \quad (48)$$

So the triangle inequality holds for TSW-SL_p . \square

C.2 Proof of Theorem D.2

Proof. We want to show for $p \geq 1$:

$$\text{MaxTSW-SL}_p(\mu, \nu) = \max_{\mathcal{L} \in \mathbb{T}} \left[W_{d_{\mathcal{L}, p}}(\mathcal{R}_{\mathcal{L}}^\alpha \mu, \mathcal{R}_{\mathcal{L}}^\alpha \nu) \right], \quad (49)$$

is a metric on $\mathcal{P}(\mathbb{R}^d)$.

Positive definiteness. For $\mu, \nu \in \mathcal{P}(\mathbb{R}^n)$, it is clear that $\text{MaxTSW-SL}_p(\mu, \mu) = 0$ and $\text{MaxTSW-SL}_p(\mu, \nu) \geq 0$. If $\text{MaxTSW-SL}_p(\mu, \nu) = 0$, then $W_{d_{\mathcal{L}, p}}(\mathcal{R}_{\mathcal{L}}^\alpha \mu, \mathcal{R}_{\mathcal{L}}^\alpha \nu) = 0$ for all $\mathcal{L} \in \mathbb{T}$. Since $W_{d_{\mathcal{L}, p}}$ is a metric, we have $\mathcal{R}_{\mathcal{L}}^\alpha \mu = \mathcal{R}_{\mathcal{L}}^\alpha \nu$ for all $\mathcal{L} \in \mathbb{T}$. But \mathbb{T} is a subset of \mathbb{L}_n^d that satisfies the condition in the remark under the proof of Theorem B.4, so we have $\mu = \nu$.

Symmetry. For $\mu, \nu \in \mathcal{P}(\mathbb{R}^n)$, we have:

$$\text{MaxTSW-SL}_p^p(\mu, \nu) = \max_{\mathcal{L} \in \mathbb{T}} \left[W_{d_{\mathcal{L}, p}}^p(\mathcal{R}_{\mathcal{L}}^\alpha \mu, \mathcal{R}_{\mathcal{L}}^\alpha \nu) \right] \quad (50)$$

$$= \max_{\mathcal{L} \in \mathbb{T}} \left[W_{d_{\mathcal{L}, p}}^p(\mathcal{R}_{\mathcal{L}}^\alpha \nu, \mathcal{R}_{\mathcal{L}}^\alpha \mu) \right] \quad (51)$$

$$= \text{MaxTSW-SL}_p^p(\nu, \mu). \quad (52)$$

So $\text{MaxTSW-SL}_p(\mu, \nu) = \text{MaxTSW-SL}_p(\nu, \mu)$.

Triangle inequality. For $\mu_1, \mu_2, \mu_3 \in \mathcal{P}(\mathbb{R}^n)$, we have:

$$\text{MaxTSW-SL}_p(\mu_1, \mu_2) + \text{TSW-SL}_p(\mu_2, \mu_3) \quad (53)$$

$$= \max_{\mathcal{L} \in \mathbb{T}} \left[W_{d_{\mathcal{L},p}}(\mathcal{R}_{\mathcal{L}}^\alpha \mu_1, \mathcal{R}_{\mathcal{L}}^\alpha \mu_2) \right] + \max_{\mathcal{L}' \in \mathbb{T}} \left[W_{d_{\mathcal{L}',p}}(\mathcal{R}_{\mathcal{L}'}^\alpha \mu_2, \mathcal{R}_{\mathcal{L}'}^\alpha \mu_3) \right] \quad (54)$$

$$\geq \max_{\mathcal{L} \in \mathbb{T}} \left[W_{d_{\mathcal{L},p}}(\mathcal{R}_{\mathcal{L}}^\alpha \mu_1, \mathcal{R}_{\mathcal{L}}^\alpha \mu_2) + W_{d_{\mathcal{L},p}}(\mathcal{R}_{\mathcal{L}}^\alpha \mu_2, \mathcal{R}_{\mathcal{L}}^\alpha \mu_3) \right] \quad (55)$$

$$\geq \max_{\mathcal{L} \in \mathbb{T}} \left[W_{d_{\mathcal{L},p}}(\mathcal{R}_{\mathcal{L}}^\alpha \mu_1, \mathcal{R}_{\mathcal{L}}^\alpha \mu_3) \right] \quad (56)$$

$$= \text{MaxTSW-SL}_p(\mu_1, \mu_3). \quad (57)$$

So the triangle inequality holds for MaxTSW-SL_p . \square

D Max Tree Sliced Wasserstein Distance on System of Lines.

Max Sliced Wasserstein distance. Max Sliced Wasserstein (MaxSW) distance [6] uses only one maximal projecting direction instead of multiple projecting directions as SW.

$$\text{MaxSW}_p(\mu, \nu) := \max_{\theta \in \mathcal{U}(\mathbb{S}^{d-1})} \left[W_p(\theta \# \mu, \theta \# \nu) \right], \quad (58)$$

MaxSW requires an optimization procedure to find the projecting direction. It is a metric on space of probability distributions on \mathbb{R}^d .

We define the Max Tree Sliced Wasserstein distance on System of Lines (MaxTSW-SL) as follows.

Definition D.1 (Max Tree-Sliced Wasserstein Distance on System of Lines). For $p \geq 1$, the *Max Tree-Sliced p -Wasserstein Distance on System of Lines* between two probability distributions μ, ν in $\mathcal{P}(\mathbb{R}^d)$ is defined by:

$$\text{MaxTSW-SL}_p(\mu, \nu) = \max_{\mathcal{L} \in \mathbb{T}} \left[W_{d_{\mathcal{L},p}}(\mathcal{R}_{\mathcal{L}}^\alpha \mu, \mathcal{R}_{\mathcal{L}}^\alpha \nu) \right], \quad (59)$$

MaxTSW-SL_p is a metric on $\mathcal{P}(\mathbb{R}^d)$. The proof of the below theorem is in Appendix C.2.

Theorem D.2. For $p \geq 1$, the *MaxTSW-SL $_p$ distance is a metric on $\mathcal{P}(\mathbb{R}^d)$.*

We provide an algorithm to compute the MaxTSW-SL in Algorithm 4.

Algorithm 3 Tree Sliced Wasserstein distance on System of Lines.

Input: Probability measures μ and ν , the number of lines in each tree system n , the number of tree systems L , a splitting function $\alpha: \mathbb{R}^d \rightarrow \Delta_n$.

Set $\widehat{\text{TSW-SL}}_1(\mu, \nu) = 0$.

for $i = 1$ to L **do**

Sampling tree system $\mathcal{L}_i = ((x_1^{(i)}, \theta_1^{(i)}), \dots, (x_n^{(i)}, \theta_n^{(i)}))$.

Projecting μ and ν onto \mathcal{L}_i to get $\mathcal{R}_{\mathcal{L}_i}^\alpha \mu$ and $\mathcal{R}_{\mathcal{L}_i}^\alpha \nu$.

Compute $\widehat{\text{TSW-SL}}_1(\mu, \nu) = \widehat{\text{TSW-SL}}_1(\mu, \nu) + (1/L) \cdot W_{d_{\mathcal{L}_i,1}}(\mathcal{R}_{\mathcal{L}_i}^\alpha \mu, \mathcal{R}_{\mathcal{L}_i}^\alpha \nu)$.

end for

Return: $\widehat{\text{TSW-SL}}_1(\mu, \nu)$.

Algorithm 4 Max Tree Sliced Wasserstein distance on a system of lines.

Input: Probability measures μ and ν , the number of lines in tree system n , a splitting function $\alpha: \mathbb{R}^d \rightarrow \Delta_n$, learning rate η , max number of iterations T
Initialize $x_1 \in \mathbb{R}^d$, $t_2, \dots, t_n \in \mathbb{R}$, $\theta_1, \dots, \theta_n \in \mathbb{S}^{d-1}$.
Compute \mathcal{L} corresponded to $(x_1, t_2, \dots, t_n, \theta_1, \dots, \theta_n)$.
while \mathcal{L} not converge or reach T **do**
 $x_1 = x_1 + \eta \cdot \nabla_{x_1} W_{d_{\mathcal{L}}, p}(\mathcal{R}_{\mathcal{L}}^\alpha \mu, \mathcal{R}_{\mathcal{L}}^\alpha \nu)$.
 for $i = 2$ to k **do**
 $t_i = T_i + \eta \cdot \nabla_{t_i} W_{d_{\mathcal{L}}, p}(\mathcal{R}_{\mathcal{L}}^\alpha \mu, \mathcal{R}_{\mathcal{L}}^\alpha \nu)$.
 end for
 for $i = 2$ to k **do**
 $\theta_i = \theta_i + \eta \cdot \nabla_{\theta_i} W_{d_{\mathcal{L}}, p}(\mathcal{R}_{\mathcal{L}}^\alpha \mu, \mathcal{R}_{\mathcal{L}}^\alpha \nu)$.
 end for
end while
Compute \mathcal{L} corresponded to $(x_1, t_2, \dots, t_n, \theta_1, \dots, \theta_n)$.
Return: $\mathcal{L}, W_{d_{\mathcal{L}}, p}(\mathcal{R}_{\mathcal{L}}^\alpha \mu, \mathcal{R}_{\mathcal{L}}^\alpha \nu)$.

E Experimental details

E.1 Gradient flows

In the gradient flows experiment, we take Gaussian as the source distribution and consider two different target measures that represent two cases: (i) 25 Gaussians (multi-modal distribution), and (ii) a Swiss-roll distribution (non-linear case) in our experiments.

We fix $L = 100$ for all baselines. For TSW-SL, we use 25 trees, each tree has 4 lines to guarantee that our methods project inputs on the same number of directions as baselines. The results are averaged over 10 runs for fair comparison.

We utilize the source code adapted from [25] for this task.

E.2 Image style transfer

This section extends our experiments to evaluate our methods against various baselines as discussed in [32]. Similar to E.1, we set $L = 100$ for all baselines and employ 25 trees and 4 lines for our TSW-SL.

The results illustrated in Figure 5 demonstrate that our novel metrics substantially reduce the Wasserstein distance of a large number of baselines. Our primary contribution is the development of a metric that effectively bridges SW and TSW, exhibiting superior performance over vanilla SW, MaxSW, and several enhanced variants of SW. This represents a significant breakthrough in the field of optimal transport and paves the way for further advancements.

We utilize the source code adapted from [34] for this task.

<https://github.com/MaheyG/SWGG.git>
<https://github.com/khainb/Quasi-SW.git>

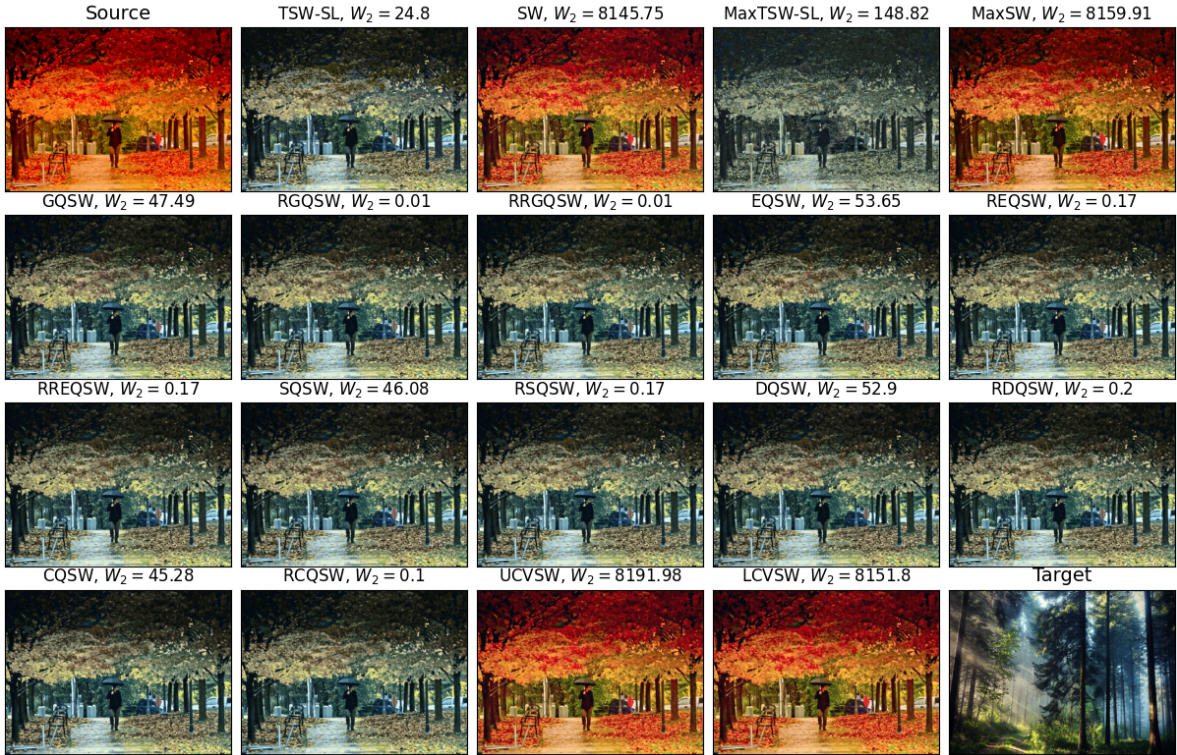


Figure 5: Style-transferred images from various baselines with 100 projecting directions.

E.3 Generative models

Architectures. We denote μ as our data distribution. Subsequently, we formulate the model distribution ν_ϕ as a resultant probability measure generated by applying a neural network G_ϕ to transform a unit multivariate Gaussian (ϵ) into the data space. Additionally, we employ another neural network T_β to map from the data space to a singular scalar value. More specifically, T_{β_1} represents the subset neural network of T_β that maps from the data space to a feature space, specifically the output of the last ResNet block, while T_{β_2} maps from the feature space (the image of T_{β_1}) to a single scalar. Formally, $T_\beta = T_{\beta_2} \circ T_{\beta_1}$. We utilize the subsequent neural network architectures for G_ϕ and T_β :

- **CIFAR10:**

- $G_\phi : z \in \mathbb{R}^{128} (\sim \epsilon : \mathcal{N}(0, 1)) \rightarrow 4 \times 4 \times 256$ (Dense, Linear) \rightarrow ResBlock up 256 \rightarrow ResBlock up 256 \rightarrow ResBlock up 256 \rightarrow BN, ReLU, \rightarrow 3×3 conv, 3 Tanh .

- $T_{\beta_1} : x \in [-1, 1]^{32 \times 32 \times 3} \rightarrow$ ResBlock down 128 \rightarrow ResBlock down 128 \rightarrow ResBlock down 128 \rightarrow ResBlock 128 \rightarrow ResBlock 128.

- $T_{\beta_2} : x \in \mathbb{R}^{128 \times 8 \times 8} \rightarrow$ ReLU \rightarrow Global sum pooling (128) \rightarrow 1 (Spectral normalization).

$$-T_\beta(x) = T_{\beta_2}(T_{\beta_1}(x)).$$

- **CelebA:**

- $G_\phi : z \in \mathbb{R}^{128} (\sim \epsilon : \mathcal{N}(0, 1)) \rightarrow 4 \times 4 \times 256$ (Dense, Linear) \rightarrow ResBlock up 256 \rightarrow ResBlock up 256 \rightarrow ResBlock up 256 \rightarrow BN, ReLU, $\rightarrow 3 \times 3$ conv, 3 Tanh .

- $T_{\beta_1} : \mathbf{x} \in [-1, 1]^{32 \times 32 \times 3} \rightarrow$ ResBlock down 128 \rightarrow ResBlock down 128 \rightarrow ResBlock down 128 \rightarrow ResBlock 128 \rightarrow ResBlock 128.

- $T_{\beta_2} : x \in \mathbb{R}^{128 \times 8 \times 8} \rightarrow$ ReLU \rightarrow Global sum pooling(128) $\rightarrow 1$ (Spectral normalization).

$$-T_\beta(x) = T_{\beta_2}(T_{\beta_1}(x)).$$

We use the following bi-optimization problem to train our neural networks:

$$\begin{aligned} & \min_{\beta_1, \beta_2} (\mathbb{E}_{x \sim \mu} [\min(0, -1 + T_\beta(x))] + \mathbb{E}_{z \sim \epsilon} [\min(0, -1 - T_\beta(G_\phi(z)))]), \\ & \min_{\phi} \mathbb{E}_{X \sim \mu^{\otimes m}, Z \sim \epsilon^{\otimes m}} \left[\mathcal{S} \left(\tilde{T}_{\beta_1, \beta_2} \# P_X, \tilde{T}_{\beta_1, \beta_2} \# G_\phi \# P_Z \right) \right], \end{aligned}$$

where the function $\tilde{T}_{\beta_1, \beta_2} = [T_{\beta_1}(x), T_{\beta_2}(T_{\beta_1}(x))]$ which is the concatenation vector of $T_{\beta_1}(x)$ and $T_{\beta_2}(T_{\beta_1}(x))$, \mathcal{S} is an estimator of the sliced Wasserstein distance.

Training setup In our experiments, we configured the number of training iterations to 100000 for CIFAR10 and 50000 for CelebA. The generator G_ϕ is updated every 5 iteration, while the feature function T_β undergoes an update each iteration. Across all datasets, we maintain a consistent mini-batch size of 128. We leverage the Adam (Kingma & Ba, 2014) optimizer with parameters $(\beta_1, \beta_2) = (0, 0.9)$ for both G_ϕ and T_β with the learning rate 0.0002. Furthermore, we employ 50000 random samples from estimated generative models G_ϕ for computing the FID and Inception scores. For FID score evaluation, the statistics of datasets are computed using all training samples.

Results For quantitative analysis, Figure 6 displays a selection of randomly generated images produced by the trained models. It is evident that utilizing our TSW-SL as the generator loss significantly enhances the quality of the generated images. Additionally, increasing the number of projections further improves the visual quality of images across all estimators. This improvement in visual quality is corroborated by the FID and IS scores presented in Table 2.

We utilize the source code adapted from [27] for this task.

E.4 Computational infrastructure

All experiments are conducted on a single NVIDIA A100 GPU. Training generative models on CIFAR10 requires 14 hours, while CelebA training takes 22 hours. Regarding gradient flows, each dataset’s experiments take precisely 3.5 hours. For image style transfer, the runtime is 15 minutes.

<https://github.com/GongXinyuu/sngan.pytorch.git>

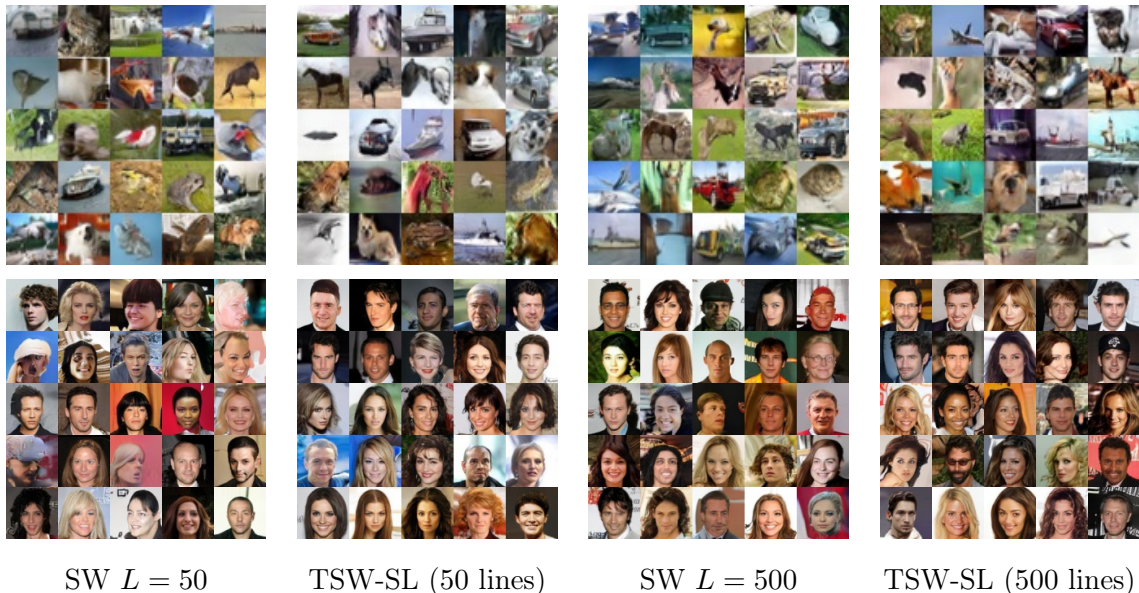


Figure 6: Randomly generated images of different methods on CIFAR10 and CelebA

F Broader Impact

The introduction of the Tree-Sliced Wasserstein distance on a System of Lines (TSW-SL) in this paper has a substantial societal impact by enhancing the precision and adaptability of optimal transport methods in various practical applications. By bridging the gap between Sliced Wasserstein (SW) and Tree-Sliced Wasserstein (TSW), TSW-SL offers a higher degree of flexibility and robustness, especially in dynamic settings. This advancement can significantly improve the performance of gradient flows, image style transfer, and generative models, leading to more efficient and effective computational tools. These improvements can drive progress in numerous fields, such as healthcare, where better image processing techniques can aid in more accurate medical imaging diagnostics, or in the arts and entertainment industry, where enhanced generative models can lead to more sophisticated and creative outputs. Furthermore, the ability to handle dynamic settings efficiently opens new possibilities for real-time data analysis and decision-making in various sectors, including finance, logistics, and environmental monitoring. Ultimately, TSW-SL contributes to making advanced computational techniques more versatile and applicable to a broader range of real-world problems, thereby fostering innovation and improving societal well-being.

References

- [1] Y. Bai, B. Schmitzer, M. Thorpe, and S. Kolouri. Sliced optimal partial transport. In *Proceedings of the IEEE/CVF Conference on Computer Vision and Pattern Recognition*, pages 13681–13690, 2023. (Cited on page 2.)
- [2] C. Bonet, N. Courty, F. Septier, and L. Drumetz. Efficient gradient flows in sliced-wasserstein space. *arXiv preprint arXiv:2110.10972*, 2021. (Cited on page 2.)
- [3] N. Bonneel, J. Rabin, G. Peyré, and H. Pfister. Sliced and radon wasserstein barycenters of measures. *Journal of Mathematical Imaging and Vision*, 51:22–45, 2015. (Cited on pages 2, 3, and 12.)
- [4] C. Bunne, L. Papaxanthos, A. Krause, and M. Cuturi. Proximal optimal transport modeling of population dynamics. In *International Conference on Artificial Intelligence and Statistics*, pages 6511–6528. PMLR, 2022. (Cited on page 1.)
- [5] N. Courty, R. Flamary, A. Habrard, and A. Rakotomamonjy. Joint distribution optimal transportation for domain adaptation. *Advances in neural information processing systems*, 30, 2017. (Cited on page 2.)
- [6] I. Deshpande, Y.-T. Hu, R. Sun, A. Pyrros, N. Siddiqui, S. Koyejo, Z. Zhao, D. Forsyth, and A. G. Schwing. Max-sliced wasserstein distance and its use for gans. In *Proceedings of the IEEE/CVF conference on computer vision and pattern recognition*, pages 10648–10656, 2019. (Cited on pages 9, 11, 12, and 25.)
- [7] I. Deshpande, Z. Zhang, and A. G. Schwing. Generative modeling using the sliced wasserstein distance. In *Proceedings of the IEEE conference on computer vision and pattern recognition*, pages 3483–3491, 2018. (Cited on pages 2 and 13.)
- [8] J. Fan, I. Haasler, J. Karlsson, and Y. Chen. On the complexity of the optimal transport problem with graph-structured cost. In *International Conference on Artificial Intelligence and Statistics*, pages 9147–9165. PMLR, 2022. (Cited on page 1.)
- [9] A. Hatcher. *Algebraic topology*. 2005. (Cited on pages 16 and 17.)
- [10] S. Helgason and S. Helgason. The radon transform on \mathbb{R}^n . *Integral Geometry and Radon Transforms*, pages 1–62, 2011. (Cited on page 22.)
- [11] M. Heusel, H. Ramsauer, T. Unterthiner, B. Nessler, and S. Hochreiter. Gans trained by a two time-scale update rule converge to a local nash equilibrium. 12 2017. (Cited on page 13.)
- [12] N. Ho, X. Nguyen, M. Yurochkin, H. H. Bui, V. Huynh, and D. Phung. Multilevel clustering via wasserstein means. In *International conference on machine learning*, pages 1501–1509. PMLR, 2017. (Cited on page 2.)
- [13] X. Hua, T. Nguyen, T. Le, J. Blanchet, and V. A. Nguyen. Dynamic flows on curved space generated by labeled data. In *Proceedings of the Thirty-Second International Joint Conference on Artificial Intelligence, IJCAI-23*, pages 3803–3811, 2023. (Cited on page 1.)

- [14] S. Kolouri, K. Nadjahi, U. Simsekli, R. Badeau, and G. Rohde. Generalized sliced wasserstein distances. *Advances in neural information processing systems*, 32, 2019. (Cited on pages 2 and 11.)
- [15] S. Kolouri, G. K. Rohde, and H. Hoffmann. Sliced wasserstein distance for learning gaussian mixture models. In *Proceedings of the IEEE Conference on Computer Vision and Pattern Recognition*, pages 3427–3436, 2018. (Cited on page 2.)
- [16] A. Krizhevsky. Learning multiple layers of features from tiny images. 2009. (Cited on page 13.)
- [17] H. Lavenant, S. Clatici, E. Chien, and J. Solomon. Dynamical optimal transport on discrete surfaces. In *SIGGRAPH Asia 2018 Technical Papers*, page 250. ACM, 2018. (Cited on page 1.)
- [18] T. Le, T. Nguyen, D. Phung, and V. A. Nguyen. Sobolev transport: A scalable metric for probability measures with graph metrics. In *International Conference on Artificial Intelligence and Statistics*, pages 9844–9868. PMLR, 2022. (Cited on pages 4 and 10.)
- [19] T. Le, M. Yamada, K. Fukumizu, and M. Cuturi. Tree-sliced variants of wasserstein distances. *Advances in neural information processing systems*, 32, 2019. (Cited on pages 2 and 4.)
- [20] L. Liu, S. Pal, and Z. Harchaoui. Entropy regularized optimal transport independence criterion. In *International Conference on Artificial Intelligence and Statistics*, pages 11247–11279. PMLR, 2022. (Cited on page 1.)
- [21] A. Liutkus, U. Simsekli, S. Majewski, A. Durmus, and F.-R. Stöter. Sliced-wasserstein flows: Nonparametric generative modeling via optimal transport and diffusions. In *International Conference on Machine Learning*, pages 4104–4113. PMLR, 2019. (Cited on page 2.)
- [22] C. Lozupone and R. Knight. Unifrac: a new phylogenetic method for comparing microbial communities. *Applied and environmental microbiology*, 71(12):8228–8235, 2005. (Cited on page 4.)
- [23] C. A. Lozupone, M. Hamady, S. T. Kelley, and R. Knight. Quantitative and qualitative β diversity measures lead to different insights into factors that structure microbial communities. *Applied and environmental microbiology*, 73(5):1576–1585, 2007. (Cited on page 4.)
- [24] M. Luong, K. Nguyen, N. Ho, R. Haf, D. Phung, and L. Qu. Revisiting deep audio-text retrieval through the lens of transportation. *arXiv preprint arXiv:2405.10084*, 2024. (Cited on page 1.)
- [25] G. Mahey, L. Chapel, G. Gasso, C. Bonet, and N. Courty. Fast optimal transport through sliced generalized wasserstein geodesics. In *Thirty-seventh Conference on Neural Information Processing Systems*, 2023. (Cited on pages 11 and 26.)

- [26] G. Mena and J. Niles-Weed. Statistical bounds for entropic optimal transport: sample complexity and the central limit theorem. In *Advances in Neural Information Processing Systems*, pages 4541–4551, 2019. (Cited on page 1.)
- [27] T. Miyato, T. Kataoka, M. Koyama, and Y. Yoshida. Spectral normalization for generative adversarial networks. In *International Conference on Learning Representations*, 2018. (Cited on pages 12 and 28.)
- [28] J. R. Munkres. *Elements of algebraic topology*. CRC press, 2018. (Cited on page 17.)
- [29] K. Nguyen, N. Barileto, and N. Ho. Quasi-monte carlo for 3d sliced wasserstein. In *The Twelfth International Conference on Learning Representations*, 2024. (Cited on pages 2 and 12.)
- [30] K. Nguyen and N. Ho. Amortized projection optimization for sliced wasserstein generative models. *Advances in Neural Information Processing Systems*, 35:36985–36998, 2022. (Cited on page 2.)
- [31] K. Nguyen and N. Ho. Energy-based sliced wasserstein distance. *Advances in Neural Information Processing Systems*, 36, 2024. (Cited on pages 1 and 2.)
- [32] K. Nguyen and N. Ho. Sliced wasserstein estimation with control variates. In *The Twelfth International Conference on Learning Representations*, 2024. (Cited on pages 11, 12, and 26.)
- [33] K. Nguyen, N. Ho, T. Pham, and H. Bui. Distributional sliced-wasserstein and applications to generative modeling. *arXiv preprint arXiv:2002.07367*, 2020. (Cited on page 2.)
- [34] T. Nguyen, Q.-H. Pham, T. Le, T. Pham, N. Ho, and B.-S. Hua. Point-set distances for learning representations of 3d point clouds. In *Proceedings of the IEEE/CVF International Conference on Computer Vision (ICCV)*, pages 10478–10487, 2021. (Cited on pages 1 and 26.)
- [35] T. D. Nguyen, B. L. Trippe, and T. Broderick. Many processors, little time: MCMC for partitions via optimal transport couplings. In *International Conference on Artificial Intelligence and Statistics*, pages 3483–3514. PMLR, 2022. (Cited on page 1.)
- [36] S. Nietert, Z. Goldfeld, and R. Cummings. Outlier-robust optimal transport: Duality, structure, and statistical analysis. In *International Conference on Artificial Intelligence and Statistics*, pages 11691–11719. PMLR, 2022. (Cited on page 1.)
- [37] J. Park, J. Lee, and K. Sohn. Bridging vision and language spaces with assignment prediction. *arXiv preprint arXiv:2404.09632*, 2024. (Cited on page 1.)
- [38] G. Peyré, M. Cuturi, et al. Computational optimal transport: With applications to data science. *Foundations and Trends® in Machine Learning*, 11(5-6):355–607, 2019. (Cited on page 1.)
- [39] T. Pham, S. Shimizu, H. Hino, and T. Le. Scalable counterfactual distribution estimation in multivariate causal models. In *Conference on Causal Learning and Reasoning (CLear)*, 2024. (Cited on page 1.)

- [40] M. Quellmalz, R. Beinert, and G. Steidl. Sliced optimal transport on the sphere. *Inverse Problems*, 39(10):105005, 2023. (Cited on page 2.)
- [41] J. Rabin, G. Peyré, J. Delon, and M. Bernot. Wasserstein barycenter and its application to texture mixing. In *International Conference on Scale Space and Variational Methods in Computer Vision*, pages 435–446, 2011. (Cited on pages 1 and 2.)
- [42] J. J. Rotman. *An introduction to algebraic topology*, volume 119. Springer Science & Business Media, 2013. (Cited on page 17.)
- [43] M. Saleh, S.-C. Wu, L. Cosmo, N. Navab, B. Busam, and F. Tombari. Bending graphs: Hierarchical shape matching using gated optimal transport. In *Proceedings of the IEEE/CVF Conference on Computer Vision and Pattern Recognition (CVPR)*, pages 11757–11767, 2022. (Cited on page 1.)
- [44] T. Salimans, I. Goodfellow, W. Zaremba, V. Cheung, A. Radford, and X. Chen. Improved techniques for training gans. NIPS’16, page 2234–2242, Red Hook, NY, USA, 2016. Curran Associates Inc. (Cited on page 13.)
- [45] C. Semple and A. Mike. Steel, phylogenetics, vol. 24. *Oxford Lecture Series in Mathematics and its Applications*. Oxford University Press, Oxford, 2003. (Cited on page 4.)
- [46] J. Solomon, F. De Goes, G. Peyré, M. Cuturi, A. Butscher, A. Nguyen, T. Du, and L. Guibas. Convolutional Wasserstein distances: Efficient optimal transportation on geometric domains. *ACM Transactions on Graphics (TOG)*, 34(4):66, 2015. (Cited on page 1.)
- [47] Y. Takezawa, R. Sato, Z. Kozareva, S. Ravi, and M. Yamada. Fixed support tree-sliced Wasserstein barycenter. In *Proceedings of The 25th International Conference on Artificial Intelligence and Statistics*, volume 151, pages 1120–1137. PMLR, 2022. (Cited on page 1.)
- [48] C. Villani. *Optimal Transport: Old and New*, volume 338. Springer Science & Business Media, 2008. (Cited on pages 1 and 3.)
- [49] J. Wang, R. Gao, and Y. Xie. Two-sample test with kernel projected Wasserstein distance. In *Proceedings of The 25th International Conference on Artificial Intelligence and Statistics*, volume 151, pages 8022–8055. PMLR, 2022. (Cited on page 1.)
- [50] J. Weed and Q. Berthet. Estimation of smooth densities in Wasserstein distance. In *Proceedings of the Thirty-Second Conference on Learning Theory*, volume 99, pages 3118–3119, 2019. (Cited on page 1.)
- [51] J. Wu, Z. Huang, D. Acharya, W. Li, J. Thoma, D. P. Paudel, and L. V. Gool. Sliced wasserstein generative models. In *Proceedings of the IEEE/CVF Conference on Computer Vision and Pattern Recognition*, pages 3713–3722, 2019. (Cited on page 2.)